December 1, 1998
Physical Review D60 (1999) Oct.1

hep-ph/9812263
MSUHEP-81010

QCD Corrections to Scalar Production via Heavy Quark Fusion at Hadron Colliders

Csaba Balázs Hong-Jian He C.–P. Yuan

Department of Physics and Astronomy, Michigan State University
East Lansing, Michigan 48824, USA †

Abstract

We recently proposed that, due to the top-quark-mass enhanced Yukawa coupling, the s-channel production of a charged scalar or pseudo-scalar from heavy quark fusion can be an important new mechanism for discovering non-standard spin-0 particles. In this work, we present the complete $O(\alpha_s)$ QCD corrections to this s-channel production process at hadron colliders, and also the results of QCD resummation over multiple soft-gluon emission. The systematic QCD-improved production and decay rates at the FermiLab Tevatron and the CERN LHC are given for the charged top-pions in the topcolor models, and for the charged Higgs bosons in the generic two Higgs doublet model. The direct extension to the production of the neutral (pseudo-)scalars via $b\bar{b}$ fusion is studied in the minimal supersymmetric standard model (MSSM) with large $\tan\beta$, and in the topcolor model with large bottom Yukawa coupling.

PACS number(s): 13.85.Ni, 12.60.Fr, 14.65.Ha, 14.80.Cp

Physical Review D60 (1999) Oct. 1 issue (in press)

†Electronic address: balazs@pa.msu.edu, hjhe@pa.msu.edu, yuan@pa.msu.edu

1. Introduction

The top quark (t), among the three generations of fermions, is the only one with a large mass as high as the electroweak scale. This makes the top the most likely place to discover new physics beyond the Standard Model (SM). In a recent study [1], two of us proposed that, due to the top-mass enhanced flavor mixing Yukawa coupling of the charm (c) and bottom (b) with a charged scalar or pseudo-scalar ($\phi^\pm$), the s-channel partonic process $c\bar{b}, \bar{c}b \to \phi^\pm$, can be an important mechanism for the production of $\phi^\pm$ at various colliders. From the leading order (LO) calculation [1], we demonstrated that the FermiLab Tevatron Run-II has the potential to explore the mass range of the charged top-pions up to about 300–350 GeV in the topcolor (TopC) models [2, 3]. In this work, we compute the complete next-to-leading order (NLO) QCD corrections to the process $q\bar{q}' \to \phi^\pm$, which includes the one-loop virtual corrections and the contributions from the additional $O(\alpha_s)$ processes,

$$q\bar{q}' \to \phi^\pm g \quad \text{and} \quad qg \to q'\phi^\pm. \tag{1}$$

The decay width and branching ratio (BR) of such a (pseudo-)scalar are also included up to NLO to estimate the event rates. The QCD resummation of multiple soft-gluon radiation is also carried out, which provides a better prediction of the transverse momentum distribution of the (pseudo-)scalar particle. We shall choose the TopC model [2] as a benchmark of our analysis. The generalization to the generic type-III two-Higgs doublet model (2HDM) [4, 5] is straightforward since the QCD-corrections are universal.[1] The direct extension to the production of neutral (pseudo-)scalars via $b\bar{b}$ fusion is studied in the Minimal Supersymmetric SM (MSSM) [6, 7] with large tanβ and in the TopC models with $U(1)$-tilted large bottom Yukawa coupling [2, 3].

2. Charged Scalar Production via Charm-Bottom Fusion

2.1. Fixed-Order Analysis up to $O(\alpha_s)$

We study charged (pseudo-)scalar production via the top-mass-enhanced flavor mixing vertex c-b-$\phi^\pm$ [1]. The corresponding Yukawa coupling can be generally defined as $\mathcal{C}_L\widehat{L}+\mathcal{C}_R\widehat{R}$ in which $\widehat{L} = (1-\gamma_5)/2$ and $\widehat{R} = (1+\gamma_5)/2$. The total cross sections for the ϕ^+ production

[1] We note that the finite part of the counter term to the q-$\bar{q}'$-$\phi^{0,\pm}$ Yukawa vertex is renormalization-scheme- and model-dependent.

at hadron colliders (cf. Fig 1) can be generally expressed as

$$\sigma\left(h_1h_2\to\phi^+X\right)=\sum_{\alpha,\beta}\int_{\tau_0}^1 dx_1\int_{\frac{\tau_0}{x_1}}^1 dx_2\left[f_{\alpha/h_1}(x_1,Q^2)f_{\beta/h_2}(x_2,Q^2)+(\alpha\leftrightarrow\beta)\right]\widehat{\sigma}^{\alpha\beta}(\alpha\beta\to\phi^+X), \tag{2}$$

where $\tau_0=m_\phi^2/S,\ x_{1,2}=\sqrt{\tau_0}\,e^{\pm y},\ m_\phi$ is the mass of $\phi^\pm$, $\sqrt{S}$ is the center-of-mass energy of the h_1h_2 collider, and $f_{\alpha/h}(x,Q^2)$ is the parton distribution function (PDF) of a parton α with the factorization scale Q. The quantity $\widehat{\sigma}^{\alpha\beta}$ is the partonic cross section and has the following LO contribution for $c\bar{b}\to\phi^+$ (cf. Fig. 1a) [1]:

$$\widehat{\sigma}^{\alpha\beta}_{\rm LO}\ =\ \delta_{\alpha c}\delta_{\beta\bar{b}}\delta(1-\widehat{\tau})\widehat{\sigma}_0\ ,\qquad \widehat{\sigma}_0\equiv\frac{\pi}{12\widehat{s}}\left(|\mathcal{C}_L|^2+|\mathcal{C}_R|^2\right), \tag{3}$$

where $\widehat{\tau}=m_\phi^2/\widehat{s}$ with $\widehat{s}$ the center-of-mass energy of the sub-process, and the terms suppressed by the small mass ratio $(m_{c,b}/m_\phi)^2$ have been ignored. Since we are interested in the inclusive production of the scalar ϕ, it is natural to choose the factorization scale Q to be its mass m_ϕ, which is of $O(10^{2-3})$ GeV and much larger than the mass of charm or bottom quark. Hence, in this work, we will treat c and b as massless partons inside proton or antiproton and perform a NLO QCD calculation with consistent sets of PDFs [8, 9, 10].

The NLO contributions are of $O(\alpha_s)$, which contain three parts: (i) the one-loop Yukawa vertex and quark self-energy corrections (cf. Fig. 1b-d); (ii) the real gluon emission in the $q\bar{q}'$-annihilations (cf. Fig. 1e); (iii) s- and t-channel gluon-quark fusions (cf. Fig. 1f-g). The Feynman diagrams coming from permutations are not shown in Fig. 1. Unlike the usual Drell-Yan type of processes (where the sum of the one-loop quark-wavefunction renormalization and vertex correction gives the ultraviolet finite result), we need to include the renormalization for the Yukawa coupling (y_j) which usually relates to the relevant quark mass (m_{q_j}), i.e., we have to add the counter term at the NLO (cf. Fig.1d) besides the contribution from the usual wavefunction renormalization $Z_{q_1q_2\phi}=\frac{1}{2}(Z_{q_1}+Z_{q_2})$ (cf. Fig.1c). This applies to the Yukawa interactions of the SM and MSSM Higgs bosons as well as the top-pions in the TopC models. It is clear that, for flavor-mixing vertex c-b-$\phi^\pm$ in the TopC model [cf. Eq. (10) below], the counter-term of the Yukawa coupling is equal to the top quark mass counter-term $\delta m_t/m_t$, which we determine from the top-quark mass renormalization in the on-shell scheme so that m_t is the pole mass of the top quark. In other cases such as in the general 2HDM (type-III) [5] and the TopC models (with b-Higgs or b-pions) [11], some of their Yukawa couplings are not related to quark masses or not of the above simple one-to-

one correspondence, and thus have their independent counter terms ($\delta y_j/y_j$). In addition to the virtual QCD-loop corrections, the contributions of the real gluon emission from the initial state quarks have to be included (cf. Fig. 1e). The soft and collinear singularities appeared in these diagrams are regularized by the dimensional regularization prescription at $D = 4 - 2\epsilon$ dimensions. After summing up the contributions of virtual gluon-loop and real gluon-radiation (cf. Fig. 1b-e), the ultraviolet and soft singularities separately cancel. The collinear singularities are still left over and should be absorbed into the renormalization of the PDF [12]. (The $\overline{\rm MS}$ renormalization scheme is used in our calculation.) Finally, the gluon-quark fusion sub-processes (cf. Fig. 1f-g) should also be taken into account and computed at general dimension-D. All these results are separately summarized into the Appendix.

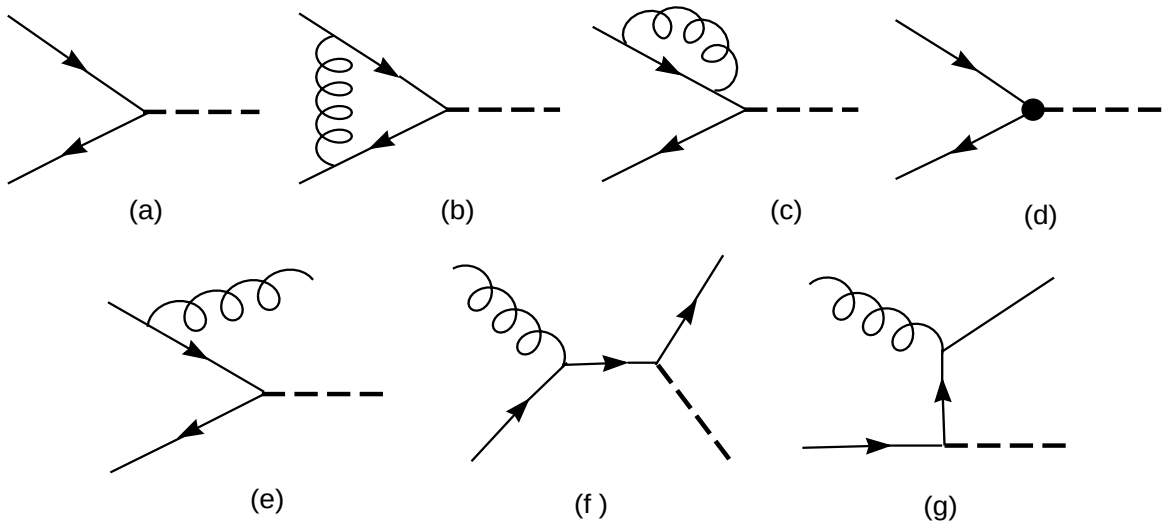

Figure 1: Representative diagrams for charged or neutral (pseudo-)scalar (dashed line) production from quark-antiquark and quark-gluon collisons at $O(\alpha_s^0)$ and $O(\alpha_s^1)$: (a) leading order contribution; (b-d) self-energy and vertex corrections (with counter term); (e) real gluon radiation in $q\bar{q}'$-fusion; (f-g) s- and t-channel gluon-quark fusions.

The hadron cross sections become regular after renormalizing the Yukawa coupling and the PDFs in (2), which are functions of the renormalization scale μ and the factorization scale $\mu_F (= \sqrt{Q^2})$. The partonic NLO cross section $\widehat{\sigma}^{\alpha\beta}_{\rm NLO}\,(\alpha\beta \to \phi^+ X)$ contains the contributions

$\Delta\widehat{\sigma}_{q\bar{q}'}(q\bar{q}' \to \phi^+,\, \phi^+ g)$, $\Delta\widehat{\sigma}_{qg}(qg \to \phi^+ q')$, and $\Delta\widehat{\sigma}_{\bar{q}g}(\bar{q}g \to \phi^+ \bar{q}')$:

$$
\begin{aligned}
&(\Delta\widehat{\sigma}_{q\bar{q}'},\ \Delta\widehat{\sigma}_{qg},\ \Delta\widehat{\sigma}_{\bar{q}g}) = \widehat{\sigma}_0 \times \frac{\alpha_s}{2\pi}\left(\delta_{qc}\delta_{\bar{q}'\bar{b}}\Delta\overline{\sigma}_{c\bar{b}},\ \delta_{qc}\Delta\overline{\sigma}_{cg},\ \delta_{\bar{q}\bar{b}}\Delta\overline{\sigma}_{\bar{b}g}\right), \\
&\Delta\overline{\sigma}_{c\bar{b}} = C_F\left[4\left(1+\widehat{\tau}^2\right)\left(\frac{\ln(1-\widehat{\tau})}{1-\widehat{\tau}}\right)_+ - 2\frac{1+\widehat{\tau}^2}{1-\widehat{\tau}}\ln\widehat{\tau} + \left(\frac{2\pi^2}{3} - 2 - \Omega\right)\delta(1-\widehat{\tau}) + 2(1-\widehat{\tau})\right] \\
&\qquad + 2P^{(1)}_{q\leftarrow q}(\widehat{\tau})\ln\frac{m_\phi^2}{Q^2}\ , \\
&\Delta\overline{\sigma}_{cg,\bar{b}g} = P^{(1)}_{q\leftarrow g}(\widehat{\tau})\left[\ln\frac{(1-\widehat{\tau})^2}{\widehat{\tau}} + \ln\frac{m_\phi^2}{Q^2}\right] - \frac{1}{4}(1-\widehat{\tau})\,(3-7\widehat{\tau})\,, \\
&P^{(1)}_{q\leftarrow q}(\widehat{\tau}) = C_F\left(\frac{1+\widehat{\tau}^2}{1-\widehat{\tau}}\right)_+, \qquad P^{(1)}_{q\leftarrow g}(\widehat{\tau}) = \frac{1}{2}\left[\widehat{\tau}^2 + (1-\widehat{\tau})^2\right],
\end{aligned}
\tag{4}
$$

where $\widehat{\tau} = m_\phi^2/\widehat{s}$ and $C_F = 4/3$. The mass counter term for the Yukawa vertex renormalization is determined in the on-shell scheme, i.e.,

$$
\frac{\delta m_t}{m_t} = -\frac{C_F\alpha_s}{4\pi}\left[3\left(\frac{1}{\epsilon} - \gamma_E + \ln 4\pi\right) + \Omega\right], \tag{5}
$$

in the TopC model. Here, the bare mass m_{t0} and the renormalized mass m_t are related by $m_{t0} = m_t + \delta m_t$ and $m_t \simeq 175\,\mathrm{GeV}$ is taken to be the top-quark pole mass. The finite part of the mass counter term is $\Omega = 3\ln\left[\mu^2/m_t^2\right] + 4$ in the TopC model, where $\Omega \geq 0$ for $\mu \geq m_t e^{-2/3} \simeq 90$ GeV. In the following, we shall choose the QCD factorization scale μ_F (set as the invariant mass $\sqrt{Q^2}$) and the renormalization scale μ to be the same as the scalar mass, i.e., $\sqrt{Q^2} = \mu = m_\phi$, which means that in (4) the factor $\ln\left(m_\phi^2/Q^2\right)$ vanishes and the quantity Ω becomes

$$
\Omega = 3\ln\left[m_\phi^2/m_t^2\right] + 4\ . \tag{6}
$$

For the case of $m_\phi \gg m_t$, the logarithmic term $\ln\left(m_\phi^2/m_t^2\right)$ becomes larger for $m_\phi \gg m_t$, and its contributions to all orders in $\alpha_s\ln\left(m_\phi^2/m_t^2\right)$ may be resummed by introducing the running Yukawa coupling $y_t(\mu)$, or correspondingly, the running mass $m_t(\mu)$. In the above formula, m_t is the pole mass ($m_t^{\rm pol} \simeq 175\,\mathrm{GeV}$) and is related to the one-loop running mass via the relation [13]

$$
m_t(\mu) = m_t(m_t^{\rm pol})\left[1 - \frac{3C_F}{4\pi}\alpha_s(\mu)\ln\frac{\mu^2}{m_t^{\rm pol}}\right], \qquad m_t(m_t^{\rm pol}) = m_t^{\rm pol}\left[1 + \frac{C_F}{\pi}\alpha_s(m_t^{\rm pol})\right]^{-1}. \tag{7}
$$

Using the renormalization group equation, one can resum the leading logarithms to all orders

in α_s [14] and obtains

$$m_t(\mu) = m_t(m_t^{\rm pol}) \left[\frac{\alpha_s(\mu)}{\alpha_s(m_t^{\rm pol})}\right]^{\frac{9C_F}{33-2n_f}}, \tag{8}$$

with $n_f = 6$ for $\mu > m_t$. Thus, to include the running effect of the Yukawa coupling, we can replace the $(m_t^{\rm pol})^2$-factor (from the Yukawa coupling) inside the square of the S-matrix element [up to $O(\alpha_s)$] by the running factor

$$m_t^2(\mu)\left\{1+2\frac{C_F\alpha_s(\mu)}{\pi}\left[1+\frac{3}{4}\ln\left(\frac{\mu}{m_t^{\rm pol}}\right)^2\right]\right\} \,=\, m_t^2(\mu)\left[1+\frac{C_F\alpha_s(\mu)}{2\pi}\Omega\right], \tag{9}$$

where the logarithmic term in the bracket $[\cdots]$ is added to avoid double-counting with the resummed logarithms inside $m_t^2(\mu)$. It is clear that this $[1+(C_F\alpha_s(\mu)/2\pi)\,\Omega]$ factor will cancel the Ω-term inside the NLO hard cross section $\Delta\widehat{\sigma}_{c\bar{b}}$ in Eq. (4) at $O(\alpha_s)$, so that the net effect of the Yukawa vertex renormalization (after the resummation of leading logarithms) is to replace the relevant tree-level on-shell quark mass (related to the Yukawa coupling) by its $\overline{\rm MS}$ running mass [cf. Eq. (8)] and remove the Ω-term in Eq. (4). When the physical scale μ (chosen as the scalar mass m_ϕ) is not much larger than m_t, the above running effect is small since the $\ln(\mu/m_t)$ factor in the Yukawa counter-term $\delta m_t/m_t$ is small. However, the case for the neutral scalar production via the $b\bar{b}$ annihilation can be different. When the loop correction to the ϕ^0-b-$\bar{b}$ Yukawa coupling contains the logarithm $\ln(\mu/m_b)$, which is much larger than $\ln(\mu/m_t)$, these large logarithms should be resummed into the running coupling, as we will do in Section 4.

In the TopC model, there are three pseudo-scalars, called top-pions, which are predicted to be light, with a mass of $O(100\sim 300)$ GeV. The relevant Yukawa interactions for top-pions, including the large t_R-c_R flavor-mixing, can be written as[2] [1]

$$\begin{aligned}\mathcal{L}_Y^{\pi_t} \;=\; -\frac{m_t\tan\beta}{v}\Big[&iK_{UR}^{tt}K_{UL}^{tt\,*}\overline{t_L}t_R\pi_t^0+\sqrt{2}K_{UR}^{tt\,*}K_{DL}^{bb}\overline{t_R}b_L\pi_t^+ + \\ &iK_{UR}^{tc}K_{UL}^{tt\,*}\overline{t_L}c_R\pi_t^0+\sqrt{2}K_{UR}^{tc\,*}K_{DL}^{bb}\overline{c_R}b_L\pi_t^+ + \text{h.c.}\Big],\end{aligned} \tag{10}$$

where $\tan\beta = \sqrt{(v/v_t)^2-1}\sim O(4\text{–}1.3)$ with the top-pion decay constant $v_t\sim O(60\text{–}150)\,\text{GeV}$, and the full vacuum expectation value (VEV) $v\simeq 246$ GeV (determined by the Fermi constant). The analysis from top-quark decay in the Tevatron $t\bar{t}$ events sets a direct lower bound

[2] As pointed out in Ref. [1], an important feature deduced from (10) is that the charged top-pion $\pi_t^\pm$ mainly couples to the right-handed top (t_R) or charm (c_R) but not the left-handed top (t_L) or charm (c_L), in contrast to the standard W-t-b coupling which involves only t_L. This makes the top-polarization measurement very useful for further discriminating the signal from the background events.

on the charged top-pion mass to be larger than about 150 GeV [15, 2]. The existing low energy LEP/SLD measurement of R_b, which slightly lies above the SM value by about 0.9σ [16], also provides an indirect constraint on the top-pion Yukawa coupling $\mathcal{C}_R^{tb} = (\sqrt{2}m_t/v)\tan\beta$ due to the one-loop contribution of charged top-pions to R_b. However, given the crude approximation in estimating the top-pion loops (with all higher order terms ignored) and the existence of many other sources of contributions associated with the strong dynamics, the indirect R_b constraint is not conclusive [2]. For instance, it was shown that the 3σ R_b bound from the one-loop top-pion correction can be fully removed if the top-pion decay constant v_t is increased by about a factor of 2 (which is the typical uncertainty of the Pagels-Stokar estimate) [2, 17]; also, the non-perturbative contributions of the coloron-exchanges can shift the R_b above its SM value [2] and tend to cancel the negative top-pion corrections. Due to these reasons, it is clear that the inconlusive R_b-bound in the TopC models should not be taken too seriously. Nevertheless, to be on the safe side, we will impose the roughly estimated R_b-constraint in our current analysis of the TopC model, by including *only* the (negative) one-loop top-pion contribution as in Ref. [17].[3] As shown in Fig. 2a, the current 3σ R_b-bound requires a smaller top-pion Yukawa coupling, $\mathcal{C}_R^{tb} \sim 1.3 - 2$ (or, $\tan\beta \sim 1.3 - 2$), for the low mass region of $m_{\pi_t^\pm} \sim 200 - 500\,\text{GeV}$. Since the top-pion decay constant v_t is related to $\tan\beta$, this also requires v_t to be around $150 \sim 100\,\text{GeV}$ for $m_{\pi_t^\pm} \sim 200 - 500\,\text{GeV}$ (cf. Fig. 2b). For comparison, the usual Pagels-Stokar estimate of v_t (by keeping only the leading logarithm but not constant terms), $v_t^2 = (N_c/8\pi^2)m_t^2 \ln\Lambda^2/m_t^2$, gives $v_t \sim 64 - 97\,\text{GeV}$ for the topcolor breaking scale $\Lambda \sim 1 - 10\,\text{TeV}$, where a typical factor of $2 \sim 3$ uncertainty in the calculation of v_t^2 is expected [2, 18]. This estimate is slightly lower than the R_b-constrained values of v_t in Fig. 2b, but is still in reasonable consistency (given the typical factor of $\sqrt{2} \sim \sqrt{3}$ error in the leading logarithmic Pagels-Stokar estimate of v_t).

In (10), $K_{UL,R}$ and $K_{DL,R}$ are defined from diagonalizing the up- and down-type quark mass matrices M_U and M_D: $K_{UL}^\dagger M_U K_{UR} = M_U^{\rm dia}$, $K_{DL}^\dagger M_D K_{DR} = M_D^{\rm dia}$, with $M_U^{\rm dia}$= diag(m_u, m_c, m_t) and $M_D^{\rm dia}$= diag(m_d, m_s, m_b). For the class-I TopC models [11], we have constructed [1] a realistic and attractive pattern of K_{UL} and K_{DL} so that the well-constrained

[3] However, it is important to keep in mind that such a rough R_b-bound is likely to over-constrain the top-pion Yukawa coupling since only the negative one-loop top-pion correction (but nothing else) is included in this estimate. A weaker R_b-bound will less reduce the top-pion Yukawa coupling and thus allow larger production rates of charged top-pions at colliders which can be obtained from our current analysis by simple re-scaling.

Cabibbo-Kobayashi-Maskawa (CKM) matrix V $(= K_{UL}^\dagger K_{DL})$ can be reproduced in the Wolfenstein-parametrization [19] and all potentially large contributions to the low energy data (such as the K-$\bar{K}$, D-$\bar{D}$ and B-$\bar{B}$ mixings and the $b \to s\gamma$ rate) can be avoided [1]. We then found that the right-handed rotation matrix K_{UR} is constrained such that its 33 and 32 elements take the values as [1]

$$K_{UR}^{tt} \simeq 0.99 - 0.94, \quad K_{UR}^{tc} \leq \sqrt{1 - {K_{UR}^{tt}}^2} \simeq 0.11 - 0.33, \tag{11}$$

which show that the t_R-c_R flavor mixing can be naturally around $10 - 30\%$.

For the current numerical analysis we consider a benchmark choice [1] based upon the above TopC model:

$$\mathcal{C}_R^{tb} = \mathcal{C}_R^{tb}(R_b \,\text{constrained}), \quad \mathcal{C}_R^{cb} = \mathcal{C}_R^{tb} K_{UR}^{tc} \simeq \mathcal{C}_R^{tb} \times 0.2, \quad \mathcal{C}_L^{tb} = \mathcal{C}_L^{cb} = 0. \tag{12}$$

It is trivial to scale the numerical results presented in this paper to any other values of $\mathcal{C}_{L,R}$ when needed. Unless specified otherwise, we use CTEQ4M PDF [20] to calculate the rates. Note that CTEQ4M PDFs are consistent with the scheme used in the current study which treats the initial state quarks as massless partons in computing the Wilson coefficient functions. The only effect of the heavy quark mass is to determine at which scale Q this heavy quark parton becomes active.[4] In our case, the scale $Q = m_\phi \gg m_c,\, m_b$.

In Fig. 3, we present the total cross sections for the charged top-pion production as functions of its mass, at the Tevatron (a $p\bar{p}$ collider at 1.8 and 2 TeV) and the LHC (a pp collider at 14 TeV). We compare the improvements by including the complete NLO results [cf. (4)] and by including the resummed running Yukawa coupling or running mass [cf. (8)]. For this purpose, we first plot the LO total cross sections with the tree-level Yukawa coupling [dash-dotted curves, cf. (3) and (12)] and with the resummed running Yukawa coupling or running mass [dotted curves, cf. (3) and (8)]; then we plot the NLO cross sections with the one-loop Yukawa coupling [dashed curves, cf. (4)] and with the resummed running Yukawa coupling or running mass [solid curves, cf. (4), (8) and (9)] . We see that at the LHC there is a visible difference between the pure LO results with tree-level Yukawa coupling (dash-dotted curves) and other NLO and/or running-coupling improved results. But at the Tevatron, the LO results with running Yukawa coupling (dotted curves) are visibly smaller than the results

[4] This is the Collins-Wilczek-Zee (CWZ) scheme [21].

in all other cases for $m_\phi > 300\,\text{GeV}$. This shows that without the complete NLO calculation, including only the running Yukawa coupling in a LO result may not always warrant a better improvement. Finally, the comparison in Fig. 3 shows that the resummed running Yukawa coupling or top-mass [cf. Eq. (8)] does not generate any significant improvement from the one-loop running. This is because the top-mass is large and $\alpha_s \ln\left(m_\phi^2/m_t^2\right)$ is small for m_ϕ up to 1 TeV. Thus, the improvement of the resummation in (8) has to come from higher order effects of $\alpha_s \ln\left(m_\phi^2/m_t^2\right)$. However, as to be shown in Sec. 4, the situation for summing over powers of $\alpha_s \ln\left(m_\phi^2/m_t^2\right)$ is different due to $m_b \ll m_t,\, m_\phi$.

Fig. 4 is to examine the individual NLO contributions to the charged top-pion production via the $q\bar{q}'$ and qg sub-processes, in comparison with the full NLO contributions.[5] The LO contributions are also shown as a reference.[6] [Here q denotes the heavy charm or bottom quark.] In this figure, there are three sets of curves for the charged top-pion production cross sections: the highest set is for the LHC ($\sqrt{S} = 14\,\text{TeV}$), the middle set is for the upgraded Tevatron ($\sqrt{S} = 2\,\text{TeV}$), and the lowest set is for the Tevatron Run I ($\sqrt{S} = 1.8\,\text{TeV}$). The LO cross sections are plotted as dotted lines while the NLO cross sections as solid ones. The dashed lines show the contributions from the $q\bar{q}'$-fusion sub-processes, and the dash-dotted lines describe the contributions from the qg-fusion sub-processes. The qg-fusion cross sections are negative and are plotted by multiplying a factor of -1, for convenience. For a quantitative comparison of the individual NLO contributions versus the full NLO results, we further plot, in Fig. 5, the ratios (called K-factors) of the different NLO contributions to the LO cross section by using the same set of CTEQ4M PDFs. The solid lines of Fig. 5 show that the overall NLO corrections to the $pp, p\bar{p} \to \phi^\pm X$ processes are positive for m_ϕ above $\sim$150 (200) GeV and lie below $\sim$15 (10)% for the Tevatron (LHC) in the relevant mass region. This is in contrast with the NLO corrections to the $W^\pm$ boson production at hadron colliders, which are always positive and as large as about 25% at the Tevatron [22]. The reason of this difference originates from the differences in the $\Delta\sigma_{q\bar{q}'}$ and $\Delta\sigma_{qg,g\bar{q}}$ for $\phi^\pm$ and $W^\pm$ production. While in the case of $W^\pm$ production the positive $\Delta\sigma_{q\bar{q}'}$ piece dominates, in the case of $\phi^\pm$ production the size of negative $\Delta\sigma_{qg,g\bar{q}}$ piece becomes comparable with that of the positive $\Delta\sigma_{q\bar{q}'}$ such that a non-trivial cancellation occurs.

[5] Unless specified, qg includes both qg and $\bar{q}g$ contributions.

[6] With the exception of Figs. 3, 8, and 12, we only show our numerical results with the resummed running Yukawa coupling or running mass.

While it is reasonable to take the renormalization and the factorization scales to be m_ϕ for predicting the inclusive production rate of ϕ^+, it is desirable to estimate the uncertainty in the rates due to different choices of PDFs. For that purpose, we examine a few typical sets of PDFs from CTEQ4, which predict different shapes of charm, bottom and gluon distributions. As shown in Table 1 and Fig. 6, the uncertainties due to the choice of PDF set are generally within $\pm 20\%$ for the relevant scalar mass ranges at both the Tevatron and the LHC.

Table 1: Cross sections in fb for charged top-pion production in the TopC model at the upgraded Tevatron and the LHC are shown, by using four different CTEQ4 PDFs. They are separately given for the LO and NLO processes, and for the $q\bar{q} \to \phi^+ X$ and $qg \to \phi^+ X$ sub-processes. At the upgraded Tevatron the top number is for $m_\phi = 200$ GeV, the middle is for $m_\phi = 300$ GeV, and the bottom is for $m_\phi = 400$ GeV. At the LHC the top number is for $m_\phi = 400$ GeV, the middle is for $m_\phi = 700$ GeV, and the lowest is for $m_\phi = 1$ TeV.

Collider	Upgraded Tevatron (2 TeV)				LHC (14 TeV)			
Process \ PDF	4A1	4M	4A5	4HJ	4A1	4M	4A5	4HJ
LO	367	382	376	387	5380	5800	6060	5890
	42.6	43.7	41.5	46.6	863	901	896	906
	6.88	7.05	6.56	8.38	235	240	232	241
NLO	370	402	412	407	5430	6080	6510	6170
	45.6	48.6	47.9	51.6	912	976	997	981
	7.70	8.21	7.89	9.56	255	266	264	268
$q\bar{q} \to \phi^+ X$	551	584	585	590	7530	8290	8740	8400
	64.5	67.4	65.5	71.7	1210	1280	1290	1290
	10.6	11.1	10.5	13.0	331	341	335	343
$qg \to \phi^+ X$	− 180	− 181	− 174	− 183	−2100	−2200	−2240	−2230
	−19.2	−18.9	−17.5	−19.9	−299	−302	−293	−303
	−2.94	−2.86	−2.59	−3.34	−76.0	−74.7	−70.6	−75.0

2.2. Analysis of Multiple Soft-Gluon Resummation

The α_s corrections to the (pseudo-)scalar production involve the contributions from the emission of virtual and real gluons, as shown in Figs. 1(b), (c) and (e). As the result of

the real gluon radiation, the (pseudo-)scalar particle will acquire a non-vanishing transverse momentum (Q_T). When the emitted gluons are soft, they generate large logarithmic contributions of the form (in the lowest order): $\alpha_s \ln^m \left(Q^2/Q_T^2\right)/Q_T^2$, where Q is the invariant mass of the (pseudo-)scalar, and $m = 0, 1$. These large logarithms spoil the convergence of the perturbative series, and falsify the $O(\alpha_s)$ prediction of the transverse momentum when $Q_T \ll Q$.

To predict the transverse momentum distribution of the produced (pseudo-)scalar, we utilize the Collins–Soper–Sterman (CSS) formalism [23], resumming the logarithms of the type $\alpha_s^n \ln^m \left(Q^2/Q_T^2\right)/Q_T^2$, to all orders n in α_s ($m = 0, ..., 2n-1$). The resummation calculation is performed along the same line as for vector boson production in Ref. [22]. Here we only give the differences from that given in Ref. [22]. But for convenience, we also list the $A^{(1)}$, $A^{(2)}$, and $B^{(1)}$ coefficients of the Sudakov exponent, which have been used in the current analysis:

$$\begin{aligned} A^{(1)}\left(C_1\right) &= C_F\,, \qquad B^{(1)}\left(C_1 = b_0, C_2 = 1\right) = -\frac{3}{2}C_F\,, \\ A^{(2)}\left(C_1 = b_0\right) &= C_F\left[\left(\frac{67}{36} - \frac{\pi^2}{12}\right)N_C - \frac{5}{18}n_f\right], \end{aligned} \tag{13}$$

where $C_F = 4/3$ is the Casimir of the fundamental representation of SU(3), $N_C = 3$ is the number of SU(3) colors, and n_f is the number of light quark flavors with masses less than Q. In the above we used the canonical values of the renormalization constants $C_1 = b_0$, and $C_2 = 1$.

To recover the $O\left(\alpha_s\right)$ total cross section, we also include the Wilson coefficients $C_{i\alpha}^{(1)}$, among which $C_{ij}^{(1)}$ differs from the vector boson production (here i denotes quark or antiquark flavors, and $\alpha = q_i$ or gluon g). Explicitly,

$$\begin{aligned} C_{jk}^{(0)}(z, b, \mu, C_1/C_2) &= \delta_{jk}\delta(1-z), \qquad C_{jg}^{(0)}(z, b, \mu, C_1/C_2) = 0, \\ C_{jk}^{(1)}(z, b, \mu, C_1/C_2) &= \delta_{jk}C_F\left\{\frac{1}{2}(1-z) - \frac{1}{C_F}\ln\left(\frac{\mu b}{b_0}\right)P_{j\leftarrow k}^{(1)}(z)\right. \\ &\qquad \left. + \delta(1-z)\left[-\ln^2\left(\frac{C_1}{b_0 C_2}e^{-3/4}\right) + \frac{\mathcal{V}}{4} + \frac{9}{16}\right]\right\}, \\ C_{jg}^{(1)}(z, b, \mu, C_1/C_2) &= \frac{1}{2}z(1-z) - \ln\left(\frac{\mu b}{b_0}\right)P_{j\leftarrow g}^{(1)}(z), \end{aligned} \tag{14}$$

where $P_{j\leftarrow g}^{(1)}$ is the $O(\alpha_s)$ gluon splitting kernels [24, 25] given in the Appendix. In the above

expressions, $\mathcal{V} = \mathcal{V}_{DY} = -8 + \pi^2$ for the vector boson production [22], and $\mathcal{V} = \mathcal{V}_{\Phi} = \pi^2$ for the (pseudo-)scalar production, when using the running mass given in Eq. (8) for the Yukawa coupling. Using the canonical values of the renormalization constants, $\ln(\mu b/b_0)$ vanishes, because $\mu = C_1/b = b_0/b$.

The only remaining difference between the resummed formulae of the vector boson and (pseudo-)scalar production is in the regular (Y) terms, which comes from the difference of the $O(\alpha_s)$ real emission amplitude squares (cf., the definitions of $\mathcal{T}_{q\overline{q}}^{-1}$ and $\mathcal{T}_{qg}^{-1}$ in Appendix C of Ref. [22] and Eqs. (22) and (25) of this paper). The non-perturbative sector of the CSS resummation (the non-perturbative function and the related parameters) is assumed to be the same as that in Ref. [22].

As described in Ref. [22], the resummed total rate is the same as the $O(\alpha_s)$ rate, when we include $C_{i\alpha}^{(1)}$ and $Y^{(1)}$, and switch from the resummed distribution to the fixed order one at $Q_T = Q$. When calculating the total rate, we have applied this matching prescription. In the case of the (pseudo-)scalar production, the matching takes place at high $Q_T \sim Q$ values, and the above matching prescription is irrelevant when calculating the total rate because the cross sections there are negligible. Thus, as expected, the resummed total rate differs from the $O(\alpha_s)$ rate only by a few percent. Since the difference of the resummed and fixed order rate indicates the size of the higher order corrections, we conclude that for inclusive (pseudo-)scalar production the $O(\alpha_s^2)$ corrections are likely much smaller than the uncertainty from the parton distribution functions (cf. Fig.5).

In Fig. 7, we present the numerical results for the transverse momentum distributions of the charged top-pions (in TopC model) and the charged Higgs bosons (in 2HDM) produced at the upgraded Tevatron and the LHC. The solid curves show the resummation prediction for the typical values of m_ϕ. The dashed curves, from the $O(\alpha_s)$ prediction, are irregular as $Q_T \to 0$. The large difference of the transverse momentum distributions between the results from the resummation and fixed-order analyses throughout a wide range of Q_T shows the importance of using the resummation prediction when extracting the top-pion and Higgs boson signals. We also note that the average value of Q_T varies slowly as m_ϕ increases and it ranges from 35 to 51 GeV for m_ϕ between 250 and 550 GeV at the 14 TeV LHC, and from 23 to 45 GeV for m_ϕ between 200 and 300 GeV at the 2 TeV Tevatron.

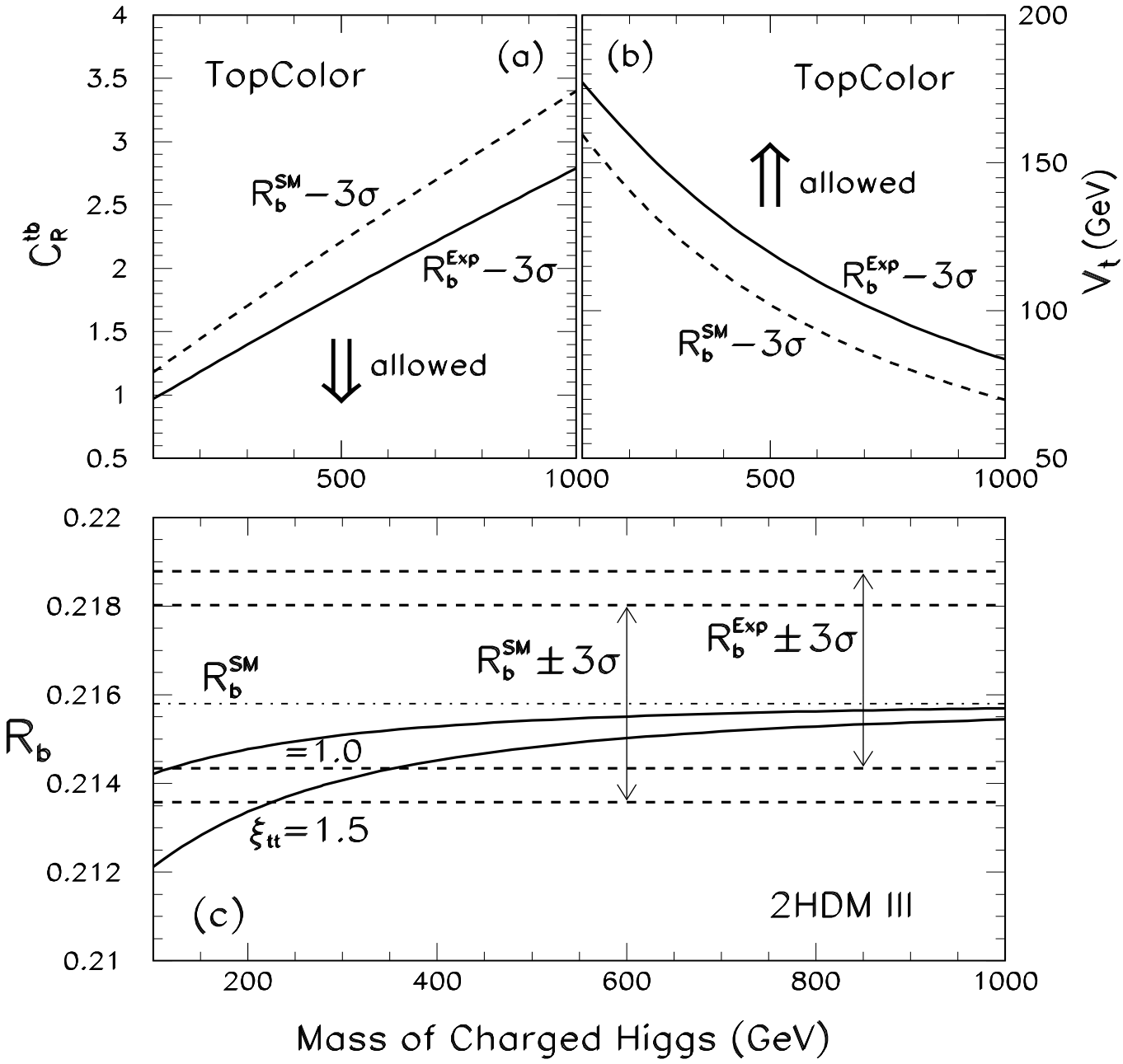

Figure 2: Estimated current 3σ-bounds in the TopC model and 2HDM-III: (a) the 3σ upper bound on the top-pion Yukawa coupling $\mathcal{C}_R^{tb}$; (b) the 3σ lower bound on the top-pion decay constant; (Here, in (a) and (b), the solid curves are derived from the combined LEP/SLD data of $R_b^{\rm Exp} = 0.21656 \pm 0.00074$ while dashed curves are from the same 3σ combined experimental error but with the central R_b-value equal to $R_b^{\rm SM} = 0.2158$.) (c) the R_b-predictions of 2HDM-III with coupling $\xi_{tt} = 1.0$ and 1.5 (solid curves) and the 3σ R_b-bounds (dashed lines).

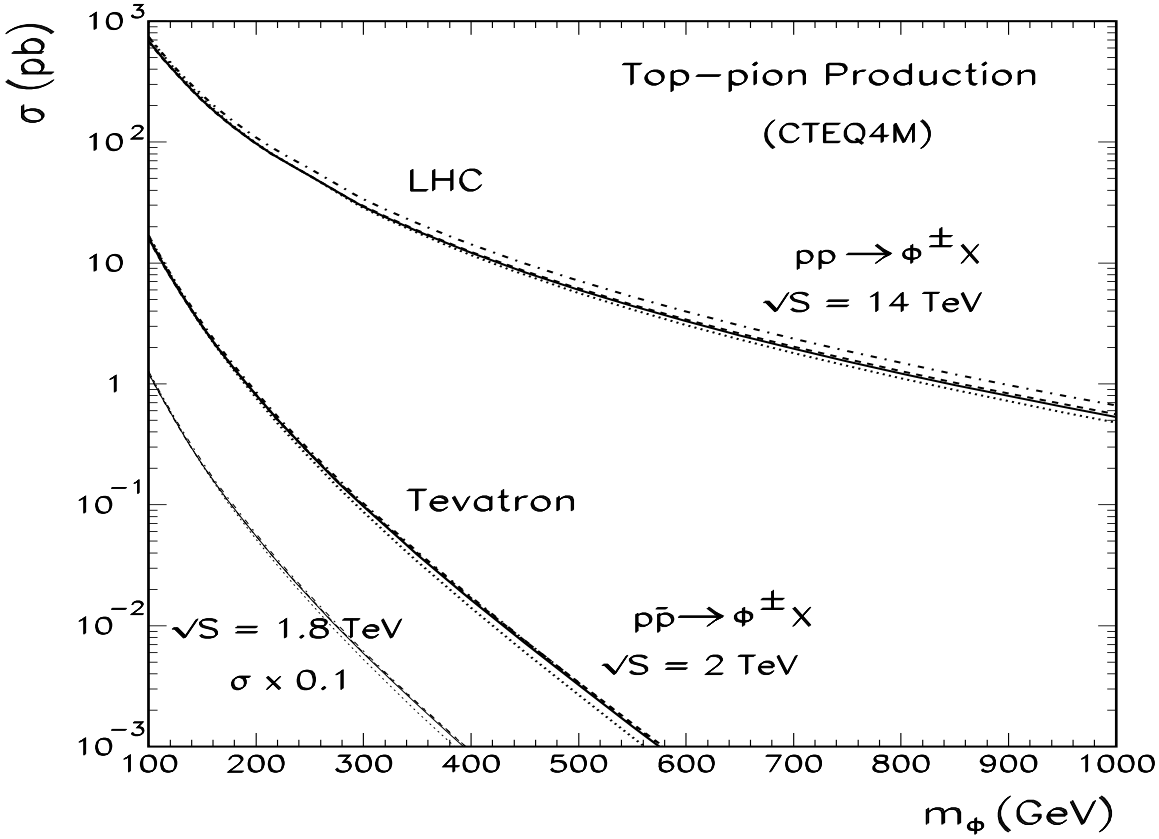

Figure 3: Top-pion production cross sections at the present Tevatron, upgraded Tevatron, and the LHC. For each collider we show the NLO cross section with the resummed running Yukawa coupling (solid), and with one-loop Yukawa coupling (dashed), as well as the LO cross section with resummed running Yukawa coupling (dotted) and with tree-level (dash-dotted) Yukawa coupling.

3. Hadronic Decays of Charged Scalars to $O(\alpha_s)$

In the TopC models, the current Tevatron data from the top quark decay into charged top-pion ($\pi_t^\pm$) and b-quark already requires the mass of $\pi_t^\pm$ to be above ∼150 GeV [2, 15]. In the current analysis, we shall consider $m_{\pi_t} > m_t + m_b$, so that its dominant decay channels are $\pi_t^\pm \to tb, cb$.

The decay width of $\pi_t^\pm$ ($= \phi^\pm$), including the $O(\alpha_s)$ QCD corrections, is given by [26, 27]:

$$
\begin{aligned}
\Gamma_{\rm NLO}(Q) &= \Gamma_{\rm LO}(Q)\left[1+\frac{\alpha_s C_F}{2\pi}\mathcal{R}\right], \\
\Gamma_{\rm LO}(Q) &= \frac{3}{16\pi}Q\left(|\mathcal{C}_L|^2+|\mathcal{C}_R|^2\right)(1-r)^2, \\
\mathcal{R} &= \frac{9}{2}(1-r)^2+(1-r)\left(3-7r+2r^2\right)\ln\frac{r}{1-r}+\left[3\ln\frac{Q^2}{m_t^2}+4-\Omega\right] \\
&\quad -2(1-r)^2\left[\frac{\ln(1-r)}{1-r}-2{\rm Li}_2\left(\frac{r}{1-r}\right)-\ln(1-r)\ln\frac{r}{1-r}\right],
\end{aligned}
\tag{15}
$$

in which $Q=\sqrt{Q^2}$ is the invariant mass of $\phi^\pm$. The small bottom and charm masses are ignored so that $r\equiv(m_t/m_\phi)^2$ for tb final state and $r=0$ for cb final state. Thus, for $\phi^\pm\to cb$, the quantity $\mathcal{R}$ reduces to $\mathcal{R}=17/2-\Omega$. In Fig. 8, we present the results for total decay widths of ϕ^+ and branching ratios of $\phi^+\to t\bar{b}$ in the TopC model and the 2HDM. For the 2HDM, we also show the branching ratios of the W^+h^0 channel, which is complementary to the $t\bar{b}$ channel. The NLO (solid) and LO (dashed) curves differ only by a small amount. In the same figure, the K-factor, defined as the ratio of the NLO to the LO partial decay widths, is plotted for the $\phi^+\to t\bar{b}$ (solid) and $\to c\bar{b}$ (dashed) channels. Here, the sample results for the 2HDM are derived for the parameter choice: $\alpha=0$ and $(M_h,\,M_A)=(100,\,1200)\,{\rm GeV}$.

With the decay width given above, we can study the invariant mass distribution of tb for the s-channel ϕ^+-production:

$$
\frac{d\sigma}{dQ^2}\left[h_1h_2\to(\phi^+X)\to t\bar{b}X\right]=\sigma\left[h_1h_2\to\phi^+(Q)X\right]\frac{(Q^2\Gamma_\phi/m_\phi)\,{\rm Br}\left[\phi^+\to t\bar{b}\right]}{\pi\left[\left(Q^2-m_\phi^2\right)^2+(Q^2\Gamma_\phi/m_\phi)^2\right]},
\tag{16}
$$

where Γ_ϕ and ${\rm Br}\left[\phi^+\to t\bar{b}\right]$ are the total decay width of ϕ^+ and the branching ratio of $\phi^+\to t\bar{b}$, respectively, which are calculated up to the NLO. We note that the one-loop box diagrams with a virtual gluon connecting the initial state quark and final state quark (from the hadronic decay of ϕ) have vanishing contribution at $O(\alpha_s)$ because the scalar ϕ is color-neutral. In Fig. 9a and Fig. 10a, we plot the invariant mass distribution for t-$\bar{b}$ and $\bar{t}$-b pairs from $\phi^\pm$ (top-pion signal) and $W^{\pm *}$ (background) decays in the TopC model. In these plots, we have included the NLO contributions, as a function of Q, to the $W^{\pm *}$ background rate at the Tevatron and the LHC. The overall K-factor (after averaging over the invariant mass Q) including both the initial and final state radiations is about 1.4 (1.34) for the Tevatron (LHC) [28]. The total rate of $W^{\pm *}$ up to the NLO is about 0.70 [0.86] pb and 11.0 pb at the 1.8 [2] TeV Tevatron and the 14 TeV LHC, respectively.

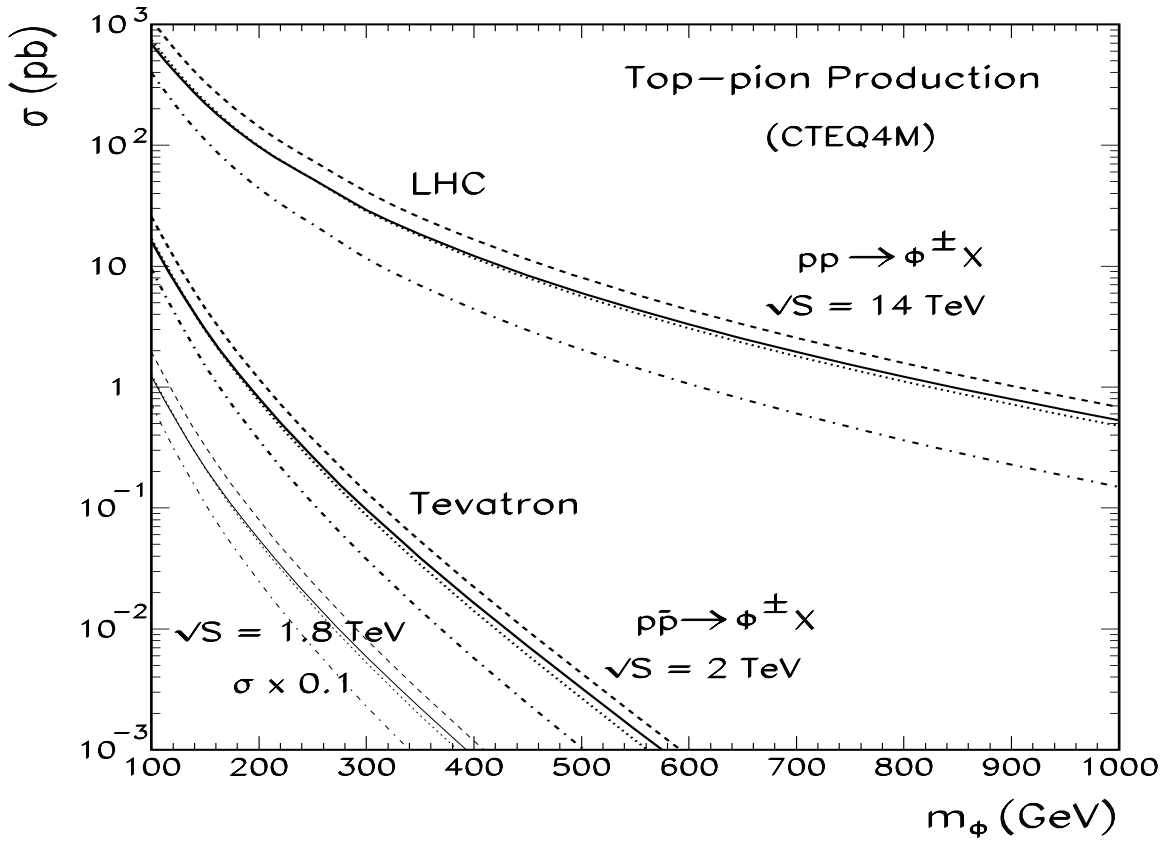

Figure 4: Cross sections for the charged top-pion production in the TopC model at the present Tevatron, upgraded Tevatron and the LHC. The NLO (solid), the $q\bar{q}'$ (dashed) and qg (dash-dotted) sub-contributions, and the LO (dotted) contributions are shown. Since the qg cross sections are negative, they are multiplied by -1 in the plot. The cross sections at $\sqrt{S} = 1.8$ TeV are multiplied by 0.1 to avoid overlap with the $\sqrt{S} = 2$ TeV curves.

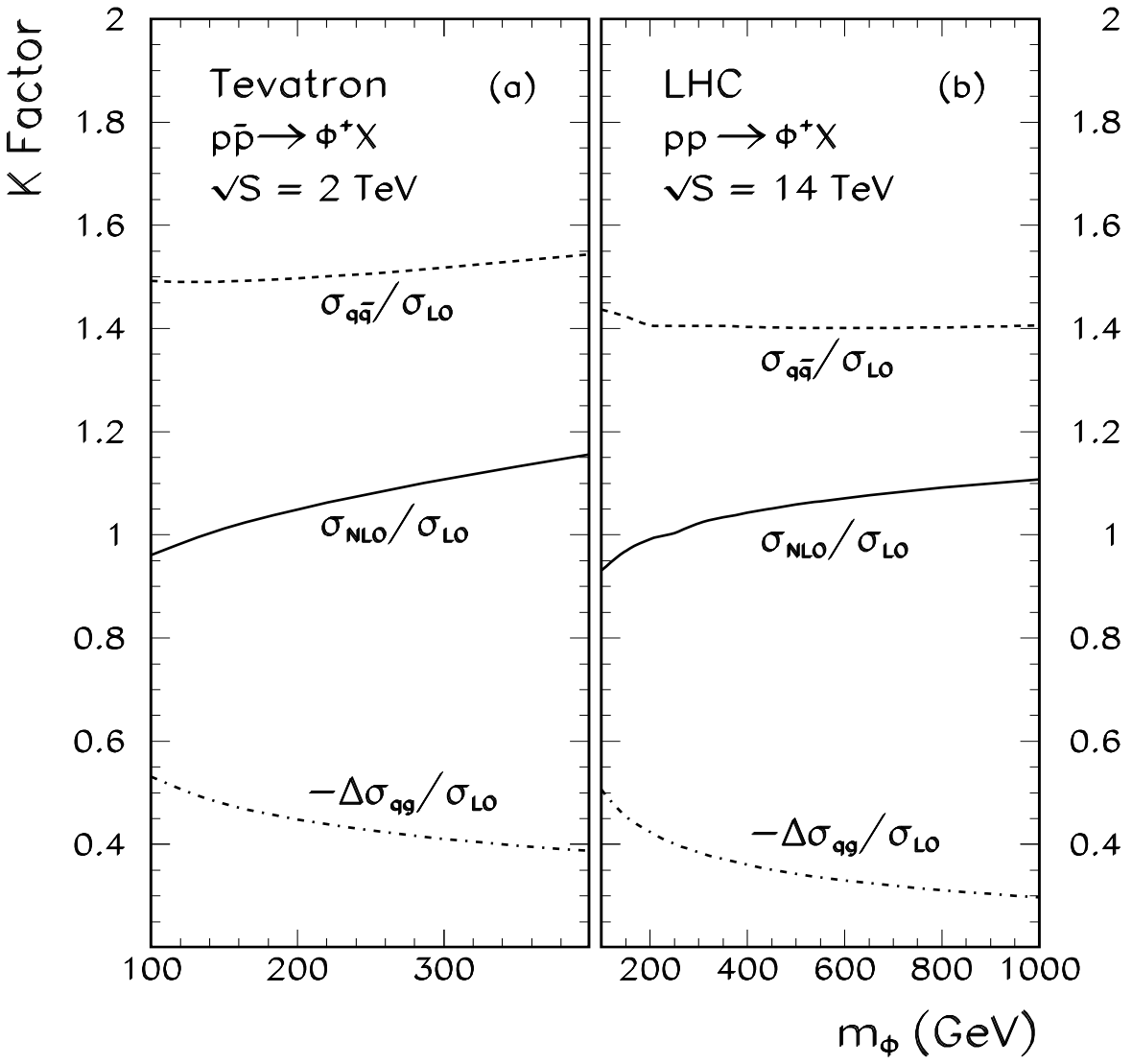

Figure 5: The K-factors for the ϕ^+ production in the TopC model are shown for the NLO ($K = \sigma_{\rm NLO}/\sigma_{\rm LO}$, solid lines), $q\bar{q}'$ ($K = \sigma_{q\bar{q}'}/\sigma_{\rm LO} = (\sigma_{\rm LO} + \Delta\sigma_{q\bar{q}'})/\sigma_{\rm LO}$, dashed lines), and qg ($K = -\Delta\sigma_{qg}/\sigma_{\rm LO}$, dash-dotted lines) contributions, at the upgraded Tevatron (a) and the LHC (b).

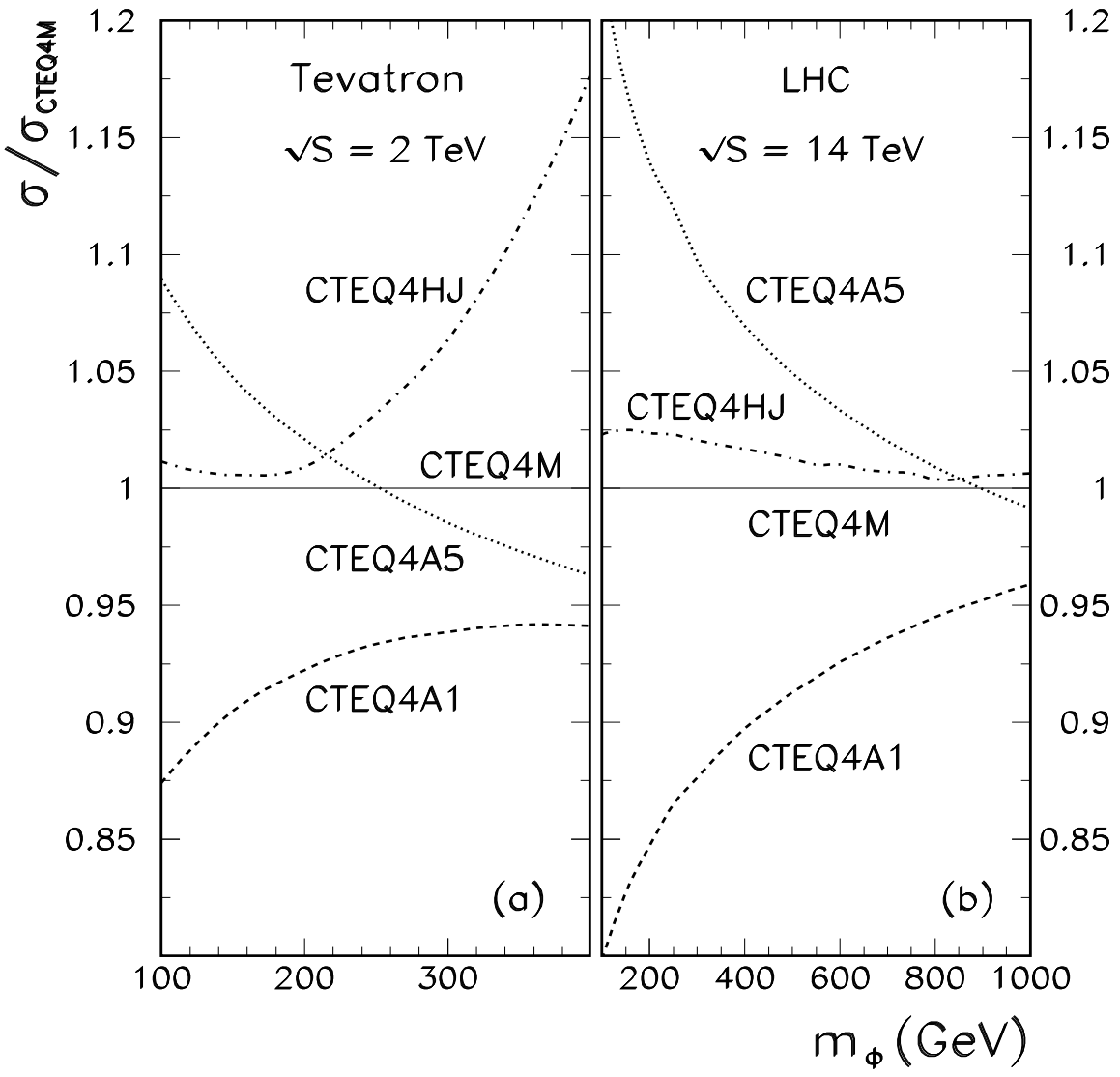

Figure 6: The ratios of NLO cross sections computed by four different sets of CTEQ4 PDFs relative to that by the CTEQ4M for charged top-pion production at the upgraded Tevatron (a) and the LHC (b).

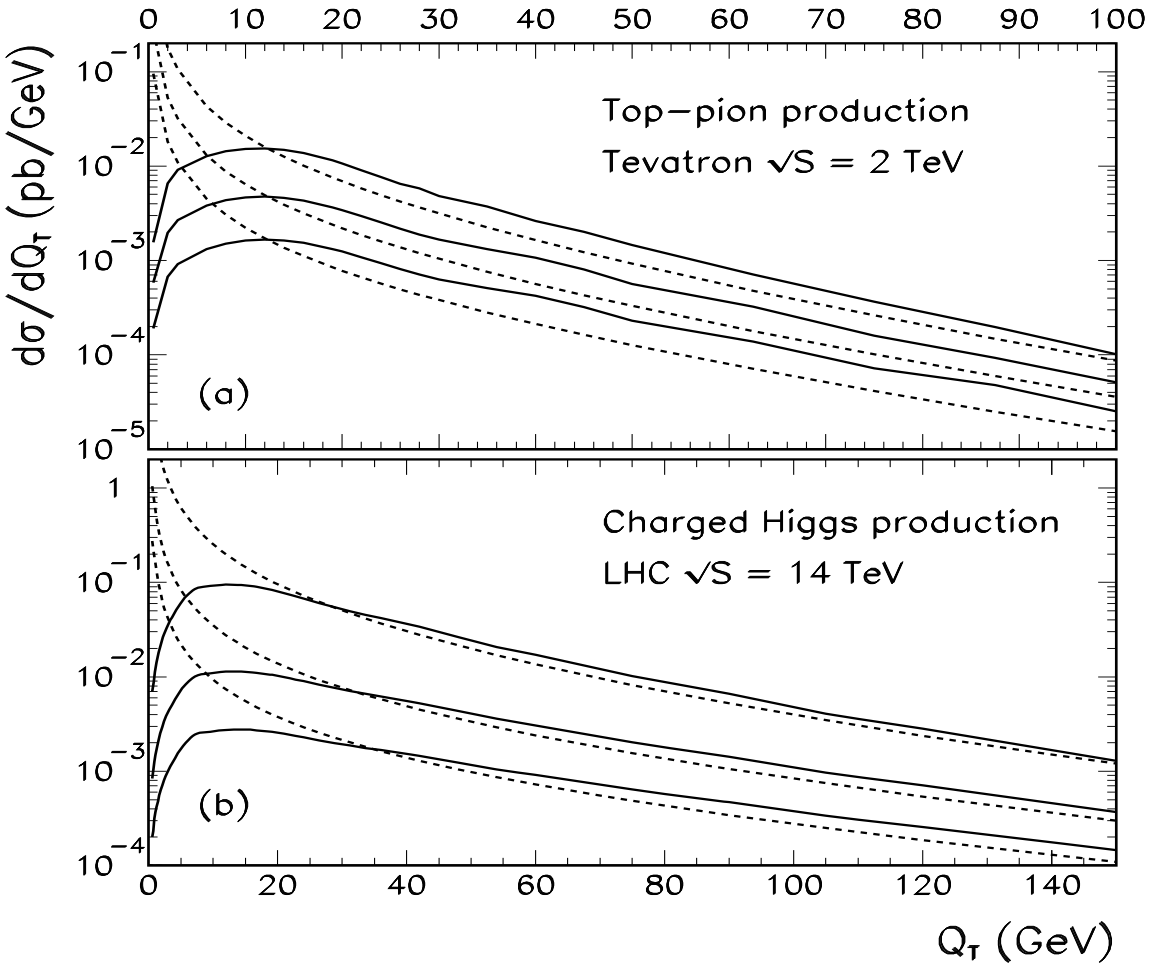

Figure 7: Transverse momentum distributions of charged top-pions produced in hadronic collisions. The resummed (solid) and $O(\alpha_s)$ (dashed) curves are calculated for $m_\phi = 200$, 250, and 300 GeV at the upgraded Tevatron (a), and for $m_\phi = 250$, 400, and 550 GeV at the LHC (b).

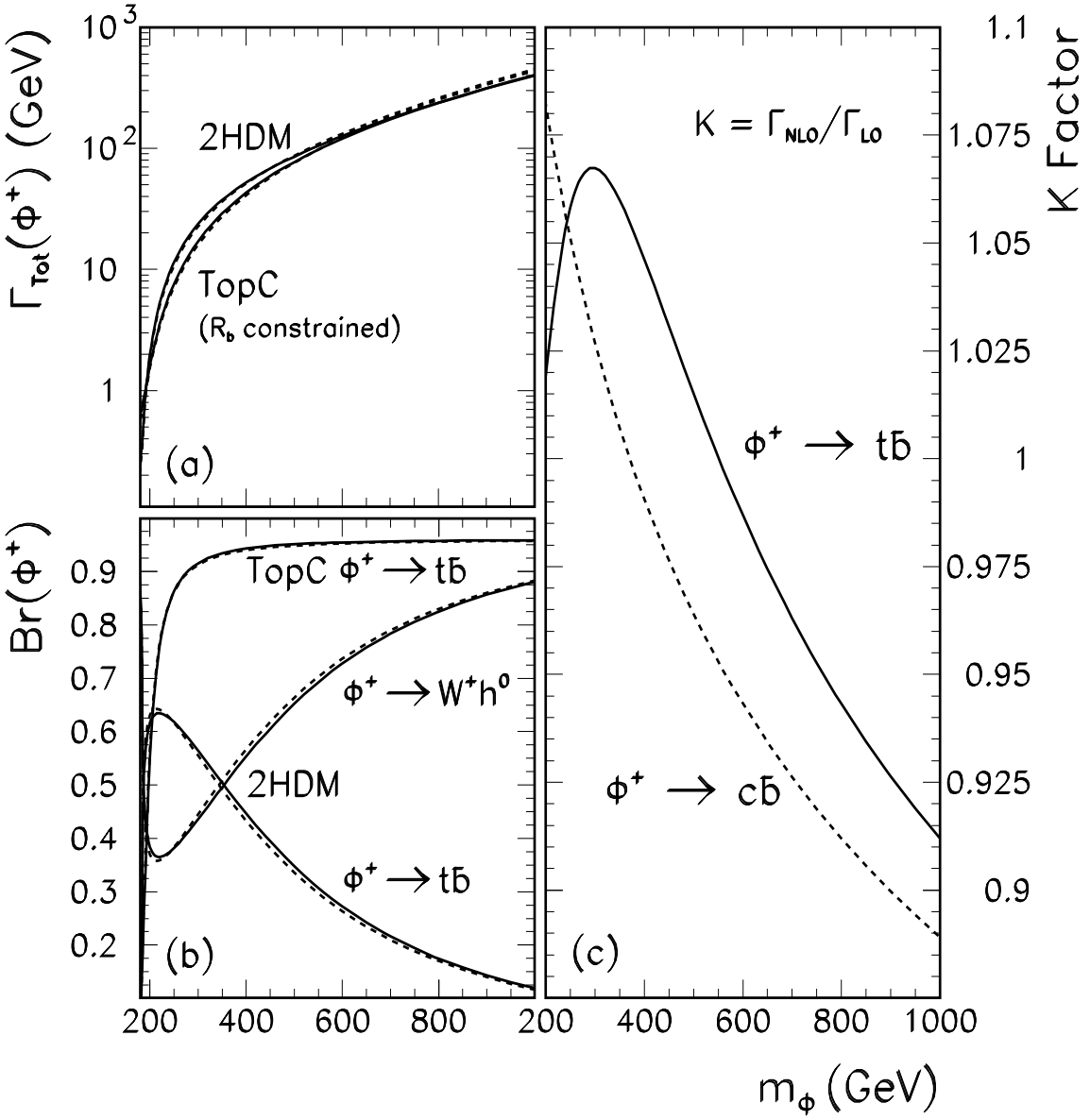

Figure 8: Total decay widths of ϕ^+ and BRs of $\phi^+ \to t\bar{b}$ in the TopC model and 2HDM. (For the 2HDM, the BR of the W^+h^0 channel is also shown, which is complementary to the $t\bar{b}$ channel.) In Fig. (a) and (b), the NLO (solid) and LO (dashed) curves differ only by a small amount. In Fig. (c), the K-factor, which is defined as the ratio of the NLO to the LO partial decay widths, is shown for the $\phi^+ \to t\bar{b}$ (solid) and $\to c\bar{b}$ (dashed) channels. The sample results for the 2HDM in this figure are derived for the parameter choice $(\xi^U_{tt},\, \xi^U_{tc}) = (1.5,\, 1.5)$, $\alpha = 0$, and $(m_h,\, m_A) = (120,\, 1200)$ GeV.

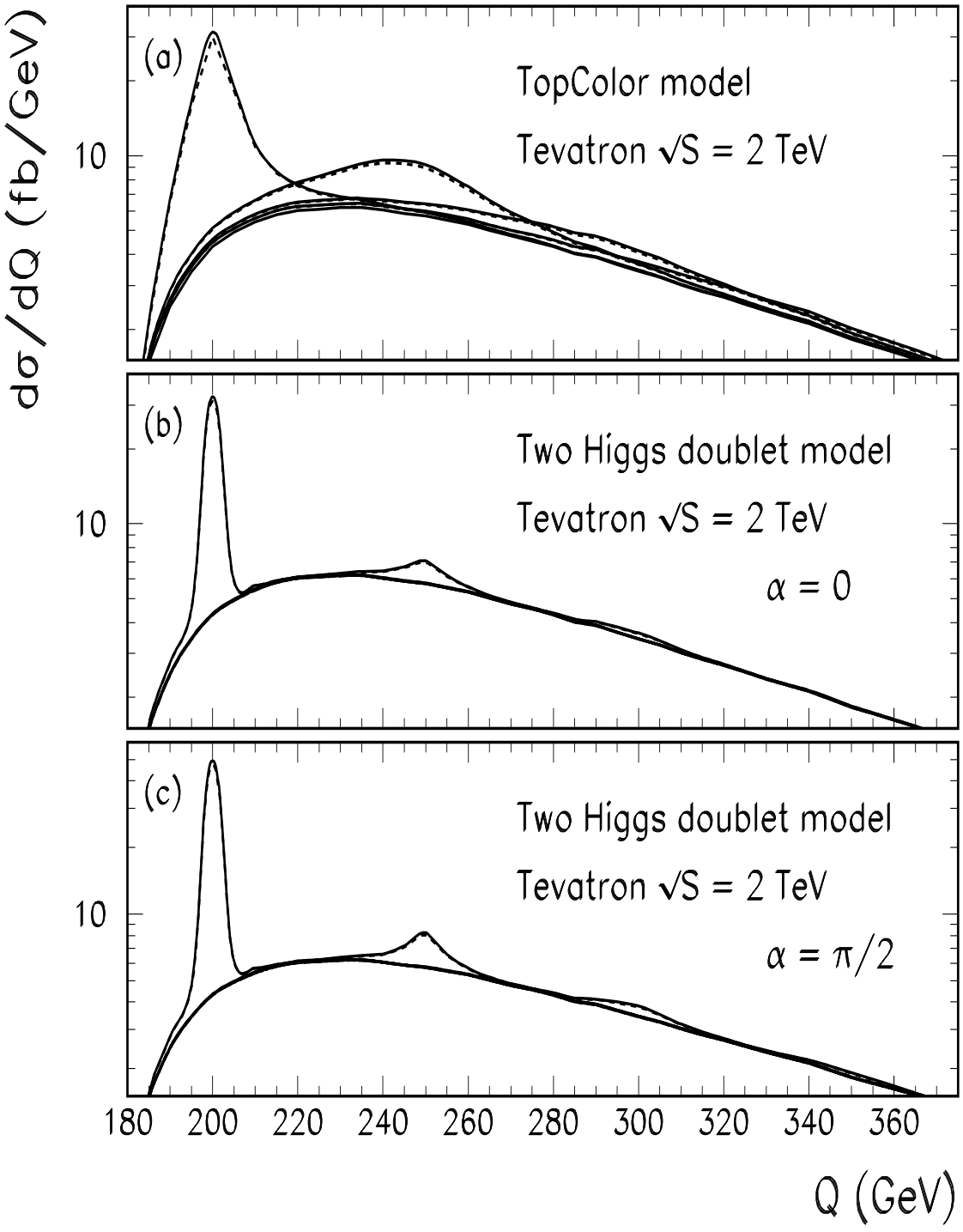

Figure 9: Invariant mass distribution of t-$\bar{b}$ and $\bar{t}$-b pairs from $\phi^{\pm}$ (signal) and $W^{\pm *}$ (background) decays at the Tevatron Run-II for the TopC model (a), and 2HDM with Higgs mixing angles $\alpha = 0$ (b), and $\alpha = \pi/2$ (c). We show the signal for $m_{\phi} = 200,\ 250,\ 300$ and $350\,\mathrm{GeV}$. The solid curves show the results from the NLO calculation, and the dashed ones from the LO analysis.

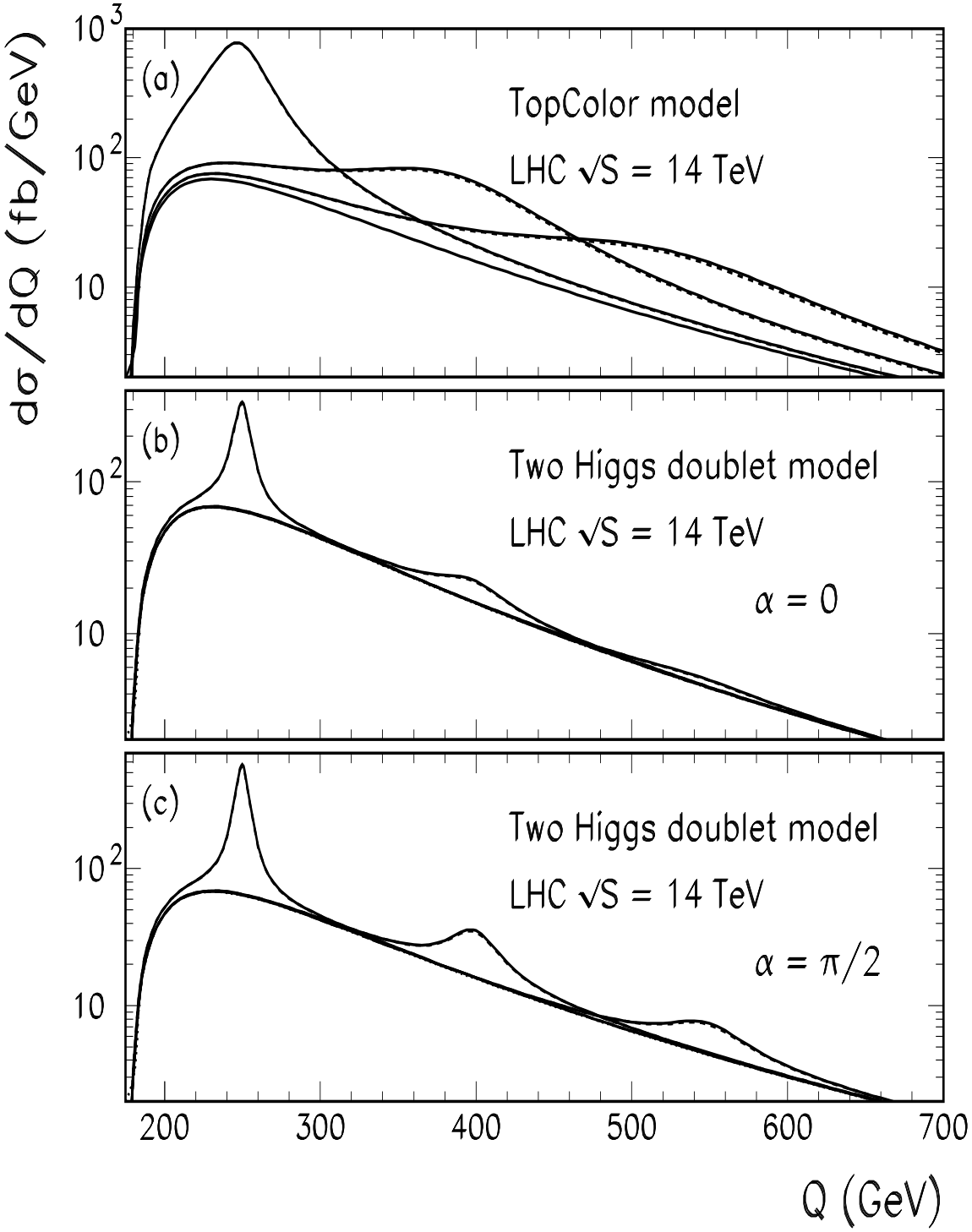

Figure 10: Invariant mass distribution of t-$\bar{b}$ and $\bar{t}$-b pairs from $\phi^{\pm}$ (signal) and $W^{\pm *}$ (background) decays at the LHC for the TopC model (a), and for the 2HDM with the Higgs mixing angles $\alpha = 0$ in (b), and $\alpha = \pi/2$ in (c). Here the charged pseudo-scalar or scalar mass are chosen as the typical values of $m_{\phi} = 250,\ 400$ and $550\,\mathrm{GeV}$. The solid curves show the results by the NLO calculation, while the dashed ones come from the LO analysis.

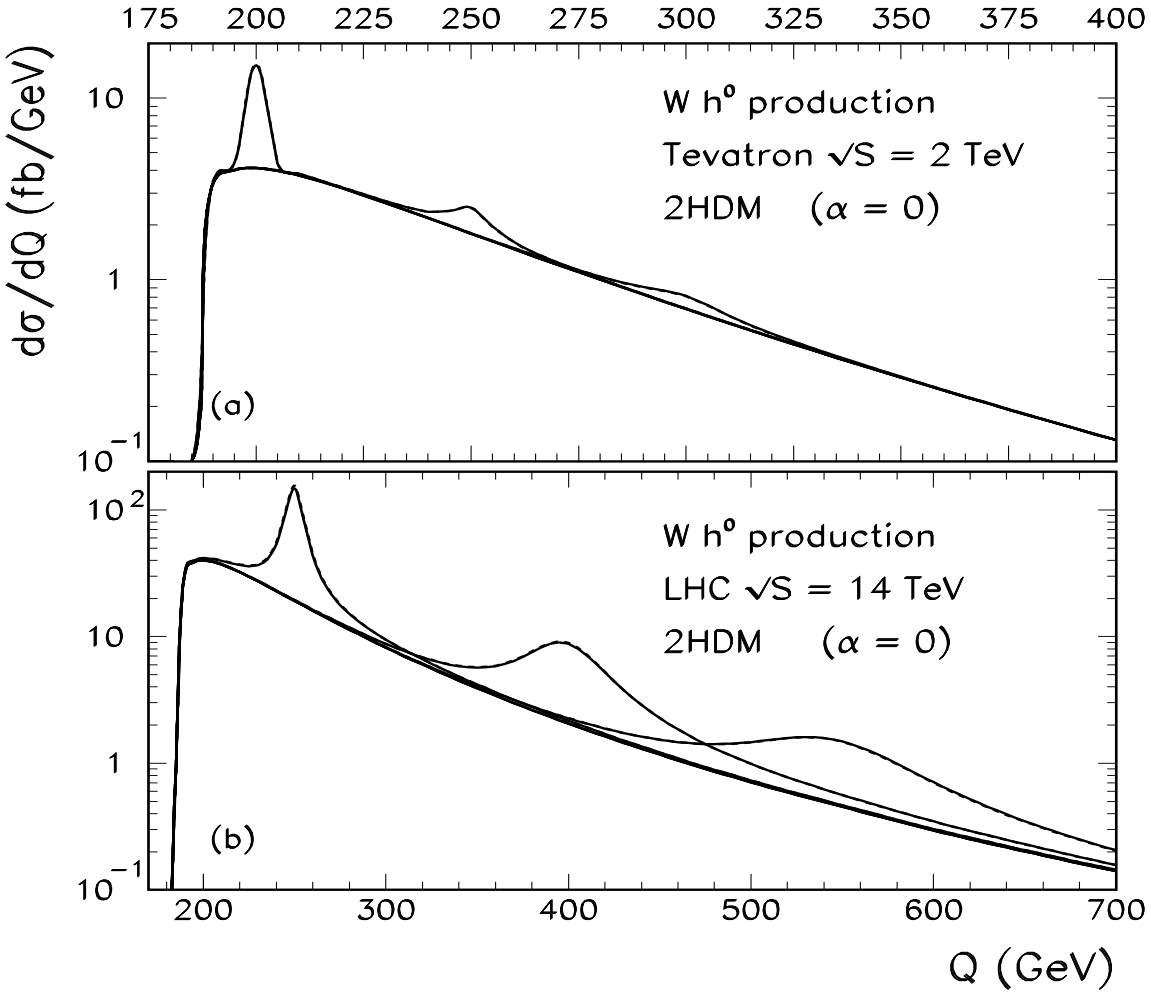

Figure 11: Invariant mass distributions of W^+-h^0 and W^--h^0 pairs from $\phi^\pm$ (s-channel resonance) and $W^{\pm *}$ (s-channel non-resonance) decays at the Tevatron Run-II, and at the LHC, for the 2HDM with Higgs mixing angles $\alpha = 0$. We show the signal for $m_\phi = 200,\ 250$ and 300 GeV at the Tevatron (a), and for $m_\phi = 250,\ 400$ and 550 GeV at the LHC (b). The solid curves show the results of the NLO calculation, and the dashed ones of the LO analysis.

Before concluding this section, we discuss how to generalize the above results to the generic 2HDM (called type-III [5]), in which the two Higgs doublets Φ_1 and Φ_2 couple to both up- and down-type quarks and the *ad hoc* discrete symmetry [29] is not imposed. The flavor-mixing Yukawa couplings in this model can be conveniently formulated under a proper basis of Higgs doublets so that $<\Phi_1>= (0, v/\sqrt{2})^T$ and $<\Phi_2>= (0,0)^T$. Thus, the diagonalization of the fermion mass matrix also diagonalizes the Yukawa couplings of Φ_1, and all the flavor-mixing effects are generated by Yukawa couplings ($\widehat{Y}^U_{ij}$ and $\widehat{Y}^D_{ij}$) of Φ_2 which exhibit a natural

hierarchy under the ansatz [4, 5]

$$\widehat{Y}^{U,D}_{ij} = \xi^{U,D}_{ij}\sqrt{m_i m_j}/<\Phi_1> \tag{17}$$

with $\xi^{U,D}_{ij} \sim O(1)$. This ansatz highly suppresses the flavor-mixings among light quarks and identifies the largest mixing coupling as the one from the t-c or c-t transition. A recent renormalization group analysis [30] shows that such a suppression persists at the high energy scales. The relevant Yukawa interactions involving the charged Higgs bosons $H^\pm$ are [1]:

$$\begin{aligned}\mathcal{L}_Y^{CC} &= H^+\left[\overline{t_R}\,(\widehat{Y}_U^\dagger V)_{tb}\,b_L - \overline{t_L}\,(V\widehat{Y}_D)_{tb}\,b_R\; + \overline{c_R}\,(\widehat{Y}_U^\dagger V)_{cb}\,b_L - \overline{c_L}\,(V\widehat{Y}_D)_{cb}\,b_R\;\right] + \text{h.c.} \\ &\simeq H^+\left[\overline{t_R}\,\widehat{Y}^{U*}_{tt}\,b_L + \overline{c_R}\,\widehat{Y}^{U*}_{tc}\,b_L\right] + \text{h.c.} + (\text{small terms})\,,\end{aligned} \tag{18}$$

where $\widehat{Y}^U_{tt} = \xi^U_{tt}\times(\sqrt{2}m_t/v) \simeq \xi^U_{tt}$, and $\widehat{Y}^U_{tc} = \xi^U_{tc}\times(\sqrt{2m_t m_c}/v) \simeq \xi^U_{tc}\times 9\%$, in which $\xi^U_{tc}\sim O(1)$ is allowed by the current low energy data [5, 32]. As a result, the Yukawa counter term in Fig. 1d involves both δm_t and δm_c. Consequently, we need to replace the NLO quantity Ω in the finite part of the Yukawa counter term [cf. the definition below (4)] by

$$\Omega(\text{2HDM}) = 3\ln\left[m^2_\phi/(m_t m_c)\right] + 4\;, \tag{19}$$

for the type-III 2HDM. In the relevant $\phi^\pm$-c-b coupling of this 2HDM, we note that, similar to the case of the TopC model, only the right-handed charm is involved [1], i.e.,

$$\mathcal{C}^{tb}_L = \mathcal{C}^{cb}_L = 0, \quad \mathcal{C}^{tb}_R = \xi^U_{tt}(\sqrt{2}m_t/v), \quad \mathcal{C}^{cb}_R \simeq \xi^U_{tc}\times 9\%. \tag{20}$$

where the parameters $(\xi^U_{tt},\,\xi^U_{tc})$ are expected to be naturally around $O(1)$. We have examined the possible constraint of ξ^U_{tt} from the current R_b data and found that the values of $\xi^U_{tt}\sim$1.0–1.5 are allowed for $m_{H^\pm} \gtrsim 200\,\text{GeV}$ (cf. Fig. 2c).[7] The production cross section of $H^\pm$ in this 2HDM can be obtained by rescaling the result of the TopC model according to the ratio of the coupling-square $\left[\mathcal{C}^{tc}_R(\text{2HDM})/\mathcal{C}^{tc}_R(\text{TopC})\right]^2 \sim \left[0.09\xi^U_{tc}/0.2\mathcal{C}^{tb}_R(\text{TopC})\right]^2$ (which is about 1/7 for $\xi^U_{tc}=1.5$ and the charged scalar mass around 400 GeV).

Finally, we note that there are three neutral Higgs bosons in the 2HDM, the CP-even scalars $(h^0,\; H^0)$ and the CP-odd pseudo-scalar A^0. The mass diagonalization for h^0 and H^0

[7] Our calculation of R_b in the 2HDM-III is consistent with those in Ref. [31] and Ref. [32] after using the same inputs. Note that a larger value of ξ^U_{tt} than ours was chosen for the solid curve in Fig. 3 of Ref. [32]. We thank L. Reina for clarifying the inputs of Ref. [32] and for useful discussions.

induces the Higgs mixing angle α. The low energy constraints on this model require [5, 32] $m_h,\, m_H \leq m_{H^\pm} \leq m_A$ or $m_A \leq m_{H^\pm} \leq m_h,\, m_H$. For the case of $m_{H^\pm} > m_{h^0} + M_W$, the $H^\pm \to W^\pm h^0$ decay channel is also open. Taking, for example, $\alpha = 0$ and $(m_h,\, m_A) = (120, 1200)\,\mathrm{GeV}$, we find from Fig. 8b that the tb and Wh^0 decay modes are complementary at low and high mass regions of the charged Higgs boson $H^\pm$. In Figs. 9b-c and 10b-c, we plot the invariant mass distributions of $t\bar{b}$ and $\bar{t}b$ pairs from $H^\pm$ (signal) and $W^{\pm *}$ (background) decays in the 2HDM at the 2 TeV Tevatron and the 14 TeV LHC, with the typical choice of the parameters: $\left(\xi^U_{tt},\, \xi^U_{tc}\right) = (1.5,\, 1.5)$ in Eq. (20), $(m_h,\, m_A) = (120,\, 1200)\,\mathrm{GeV}$, and $\alpha = 0$ or $\pi/2$. [A larger value of ξ^U_{tt} will simutaneously increase (reduce) the BR of tb (Wh^0) mode.] We see that, due to a smaller c-b-$H^\pm$ coupling [cf. (20)], it is hard to detect such a charged Higgs boson with mass $m_{H^\pm} > 250\,\mathrm{GeV}$ at the Tevatron Run-II. We then examine the potential of the LHC for the high mass range of $H^\pm$. Similar plots are shown in Figs. 9b-c for $\alpha = 0$ and $\alpha = \pi/2$, respectively. When $\cos\alpha$ is large (e.g., $\alpha = 0$), the branching ratio of the tb-channel decreases as $m_{H^\pm}$ increases (cf. Fig. 8b), so that the LHC does not significantly improve the probe of the large $m_{H^\pm}$, range via the single-top mode (cf. Fig. 10b). In this case, the $W^\pm h^0$ channel, however, becomes important for large $m_{H^\pm}$, as shown in Fig. 11 (cf. Fig. 8b, for its decay branching ratios) since the $H^\pm$-$W^\mp$-h^0 coupling is proportional to $\cos\alpha$ [5]. On the other hand, for the parameter space with small $\cos\alpha$ (e.g., $\alpha = \pi/2$), the $W^\pm h^0$ channel is suppressed so that the single-top mode is important even for large mass region of $H^\pm$.[8] This is illustrated in Fig. 10c at the LHC for $\alpha = \pi/2$. In order to probe the whole parameter space and larger $m_{H^\pm}$, it is important to study both tb and Wh^0 (or WH^0) channels.

4. Generalization to Neutral Scalar Production via $b\bar{b}$ Fusion

The QCD corrections are universal so that the generalization to the production of neutral scalar or pseudo-scalar ϕ^0 via the $b\bar{b}$ fusion is straightforward, i.e., we only need to replace (19) by

$$\Omega(\phi^0 b\bar{b}) = 3\ln\left[m^2_\phi/m^2_b\right] + 4\,, \tag{21}$$

in which m_ϕ is the mass of ϕ^0. The finite piece of the Yukawa renormalization [cf. the quantity

[8] Note that the $H^\pm$-$W^\mp$-H^0 coupling is proportional to $\sin\alpha$ and is thus enhanced for small $\cos\alpha$. In this case, the WH^0 mode may be important provided that H^0 is relatively light. We will not further elaborate this point here since it largely depends on the mass of H^0.

Ω in (5)] is scheme-dependent. We can always define the ϕ^0-b-$\bar{b}$ Yukawa coupling as $\sqrt{2}m_b/v$ times an enhancement factor K so that the Yukawa counter term is generated by $\delta m_b/m_b$.[9] After resumming the leading logarithmic terms, $\left[\alpha_s \ln(m_\phi^2/m_b^2)\right]^n$, via the renormalization group technique, the net effect of the Yukawa renormalization is to change the Yukawa coupling or the related quark-mass into the corresponding $\overline{\rm MS}$ running coupling or mass, as discussed in the previous section.

The $b\bar{b}$ decay branching ratios of the neutral Higgs bosons in the MSSM with large tanβ are almost equal to one [34]. The same is true for the b-Higgs or b-pion in the TopC model [2]. It has been shown that at the Tevatron, the $b\bar{b}$ dijet final states can be properly identified [35]. The same technique developed for studying the resonance of the coloron or techni-ρ in the $b\bar{b}$ decay mode [35] can also be applied to the search of the neutral Higgs bosons with large bottom Yukawa coupling. When the neutral scalar or pseudo-scalar ϕ^0 is relatively heavy, e.g., in the range of $O(250-1000)$ GeV, the QCD dijet backgrounds can be effectively removed by requiring the two b-jets to be tagged with large transverse momenta (P_T) because the P_T of each b-jet from the ϕ^0 decay is typically at the order of $m_\phi/2$. Hence, this process can provide complementary information to that obtained from studying the $\phi^0 b\bar{b}$ associate production [36, 33, 37].

We first consider the production of the neutral Higgs boson ϕ^0, which can be either A^0, h^0, or H^0, in the MSSM with large tanβ, where the corresponding Yukawa couplings to $b\bar{b}$ and $\tau^+\tau^-$ are enhanced relative to that of the SM since $y_D/y_D^{\rm SM}$ is equal to tanβ, $-\sin\alpha/\cos\beta$, or $\cos\alpha/\cos\beta$, respectively, at the tree-level. In the large tanβ region, the MSSM neutral Higgs bosons dominantly decay into $b\bar{b}$ and $\tau^+\tau^-$ final states, which can be detected at the hadron colliders. In comparison with the recent studies on the $\phi^0 b\bar{b}$ [33] and $\phi^0\tau^+\tau^-$ [38] associate production, we expect the inclusive ϕ^0 production via the $b\bar{b}$-fusion would be more useful for m_ϕ being relatively heavy (e.g., $m_\phi \geq 200-300$ GeV) because of the much larger phase space as well as a better suppression of the backgrounds in the high P_T region. The total LO and NLO cross sections for the inclusive production process $pp, p\bar{p} \to A^0 X$ at the Tevatron and the LHC are shown in Figs. 12a and b, in parallel to Figs. 3 and 4 for the case of charged top-pion production. Here, we have chosen tan$\beta = 40$

[9] This specific definition works even if the Yukawa coupling is not related to any quark mass. For instance, the bottom Yukawa couplings of the b-Higgs and b-pion in the TopC model [2, 33] are independent of quark masses because the b-Higgs does not develop VEV.

for illustration. The cross sections at other values of tanβ can be obtained by multiplying the scaling factor $(\tan\beta/40)^2$. From Fig. 12a, we see a significant improvement from the pure LO results (dash-dotted curves) by resumming over the large logarithms of m_ϕ^2/m_b^2 into the running Yukawa coupling. The good agreement between the LO results with running Yukawa coupling and the NLO results is due to a non-trivial, and process-dependent, cancellation between the individual $O(\alpha_s)$ contributions of the $b\bar{b}$ and bg sub-processes. In contrast to the production of the charged top-pion or Higgs boson via the initial state $c\bar{b}$ or $\bar{c}b$ partons, the neutral Higgs boson production involves the $b\bar{b}$ parton densities. The K-factors for the ratios of the NLO versus LO cross sections of $p\bar{p}/pp \to A^0X$ are presented in Fig. 13 for the MSSM with $\tan\beta = 40$. The main difference is due to the fact that the individual contribution by the $O(\alpha_s)$ bg-fusion becomes more negative as compared to the case of the charged top-pion production shown in Fig. 5. This makes the overall K-factor of the NLO versus LO cross sections range from about $-(16\sim17)\%$ to $+5\%$ at the Tevatron and the LHC. In parallel to Table 1 and Fig. 6, we have examined the uncertainties of the CTEQ4 PDFs for the A^0-production at the Tevatron and the LHC, and the results are summarized in Table 2 and Fig. 14). We also note that, similar to the charged Higgs boson production, the resummed total rate for the neutral Higgs boson production is not very different from its NLO rate.

The transverse momentum (Q_T) distributions of A^0, produced at the upgraded Tevatron and at the LHC, are shown in Fig. 15 for various A^0 masses (m_A) with $\tan\beta = 40$. The solid curves are the result of the multiple soft-gluon resummation, and the dashed ones are from the $O(\alpha_s)$ calculation. The shape of these transverse momentum distributions is similar to that of the charged top-pion (cf. Fig. 7). The fixed order distributions are singular as $Q_T \to 0$, while the resummed ones have a maximum at some finite Q_T and vanish at $Q_T = 0$. When Q_T becomes large, of the order of m_A, the resummed curves merge into the fixed order ones. The average resummed Q_T varies between 25 and 30 (40 and 60) GeV in the mass range of m_A from 200 to 300 (250 to 550) GeV at the Tevatron (LHC).

We also note that for large tanβ, the SUSY correction to the running ϕ^0-b-$\bar{b}$ Yukawa coupling is significant [39] and can be included in a way similar to our recent analysis of the $\phi^0 b\bar{b}$ associate production [33]. To illustrate the SUSY correction to the b-Yukawa coupling, we choose all MSSM soft-breaking parameters as 500 GeV, and the Higgs mixing parameter $\mu = \pm 500$ GeV. Depending on the sign of μ, the SUSY correction to the ϕ^0-b-$\bar{b}$ coupling can

either take the same sign as the QCD correction or have an opposite sign [33]. In Fig. 12c, the solid curves represent the NLO cross sections with QCD correction alone, while the results including the SUSY corrections to the running bottom Yukawa coupling are shown for $\mu = +500\,\text{GeV}$ (upper dashed curves) and $\mu = -500\,\text{GeV}$ (lower dashed curves). As shown, these partial SUSY corrections can change the cross sections by about a factor of 2. The above results are for the inclusive production of the CP-odd Higgs boson A^0 in the MSSM. Similar results can be easily obtained for the other neutral Higgs bosons (h^0 and H^0) by properly rescaling the coupling strength. We also note that in the large tanβ region, there is always a good mass-degeneracy between either h^0 and A^0 (in the low mass region with $m_A \lesssim 120\,\text{GeV}$) or H^0 and A^0 (in the high mass region with $m_A \gtrsim 120\,\text{GeV}$), as shown in Figs. 10 and 11 of Ref. [33].

Table 2: Cross sections in fb for neutral Higgs boson production in the MSSM with $\tan\beta = 40$, at the upgraded Tevatron and the LHC, are shown for four different CTEQ4 PDFs. They are separately given for the LO and NLO processes, and for the $b\bar{b} \to A^0X$ and $bg \to A^0X$ sub-processes. For the upgraded Tevatron the top number is for $m_A = 200$ GeV, the middle is for $m_A = 300$ GeV, and the lowest is for $m_A = 400$ GeV. For the LHC the top number is for $m_A = 400$ GeV, the middle is for $m_A = 700$ GeV, and the lowest is for $m_A = 1$ TeV.

Collider	Upgraded Tevatron (2 TeV)				LHC (14 TeV)			
Process \ PDF	4A1	4M	4A5	4HJ	4A1	4M	4A5	4HJ
LO	2020	1900	1660	1920	18100	19800	16600	17900
	166	153	129	163	1520	1440	1280	1440
	19.9	18.2	15.0	21.7	258	238	206	238
NLO	1810	1780	1620	1800	17100	17400	16700	17500
	160	154	134	164	1520	1470	1350	1470
	20.3	19.3	16.4	22.9	265	250	222	251
$q\bar{q} \to \phi^0 X$	3040	2900	2590	2930	25400	25400	24100	25600
	253	237	203	251	2140	2050	1850	2050
	31.0	28.8	24.0	33.8	364	339	298	340
$qg \to \phi^0 X$	−1230	−1120	−970	−1130	−8320	−8010	−7370	−8050
	−92.9	−83.1	−69.0	−87.5	−623	−575	−505	−574
	−10.6	−9.42	−7.59	−10.9	−98.8	−88.8	−75.8	−88.7

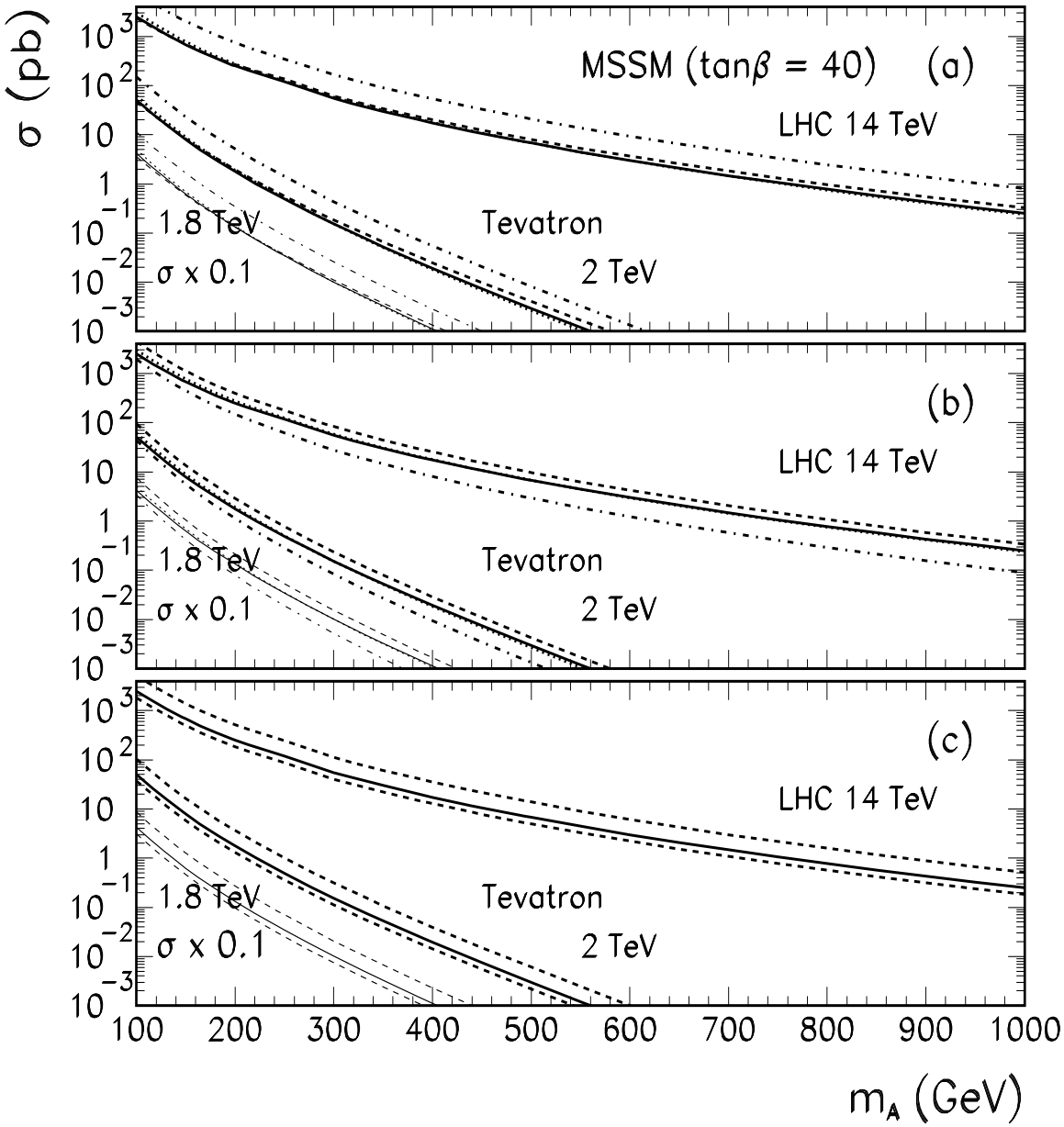

Figure 12: LO and NLO cross sections for the neutral Higgs A^0 production in the MSSM with $\tan\beta = 40$, at the Tevatron and the LHC. (a) For each collider we show the NLO cross sections with the resummed running Yukawa coupling (solid) and with one-loop Yukawa coupling (dashed), as well as the LO cross sections with resummed running Yukawa coupling (dotted) and with tree-level Yukawa coupling (dash-dotted). (b) The NLO (solid), the $b\bar{b}$ (dashed) and bg (dash-dotted) sub-contributions, and the LO (dotted) contributions are shown. Since the bg cross sections are negative, they are multiplied by -1 in the plot. The cross sections at $\sqrt{S} = 1.8$ TeV are multiplied by 0.1 to avoid overlap with the $\sqrt{S} = 2$ TeV curves. (c) The NLO cross sections with QCD running Yukawa coupling (solid curves) and those with additional SUSY correction to the running coupling are shown (upper dashed lines for the Higgs-mixing parameter $\mu = +500\,\mathrm{GeV}$ and lower dashed lines for $\mu = -500\,\mathrm{GeV}$).

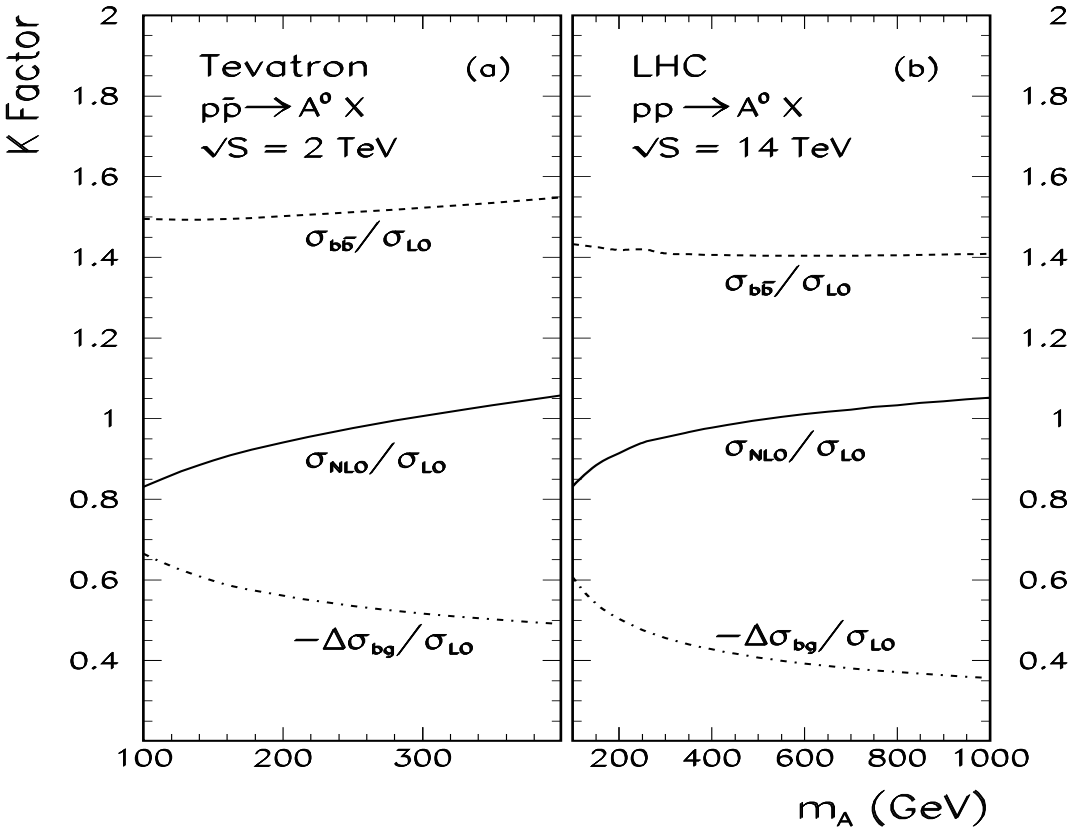

Figure 13: The K-factors for the A^0 production in the MSSM with $\tan\beta = 40$ are shown for the NLO ($K = \sigma_{\rm NLO}/\sigma_{\rm LO}$, solid lines), $b\bar{b}$ ($K = \sigma_{b\bar{b}}/\sigma_{\rm LO} = (\sigma_{\rm LO} + \Delta\sigma_{b\bar{b}})/\sigma_{\rm LO}$, dashed lines), and bg ($K = -\Delta\sigma_{bg}/\sigma_{\rm LO}$, dash-dotted lines) contributions, at the upgraded Tevatron (a) and the LHC (b).

We then consider the large bottom Yukawa coupling of the neutral b-Higgs (h_b^0) and b-pion (π_b^0) in the TopC model [2, 11, 33]. The new strong $U(1)$ force in this model is attractive in the $<\bar{t}t>$ channel but repulsive in the $<\bar{b}b>$ channel. Thus, the top but not the bottom acquires dynamical mass from the vacuum. This makes the t-Yukawa coupling (y_t) super-critical while the b-Yukawa coupling (y_b) sub-critical, at the TopC breaking scale Λ, i.e., $y_b(\Lambda) \stackrel{<}{\sim} y_{\rm crit} = \sqrt{8\pi^2/3} \stackrel{<}{\sim} y_t(\Lambda)$, which requires y_b being close to y_t and thus naturally large. Our recent renormalization group analysis [33] shows that the relation $y_b(\mu)\sim y_t(\mu)$ holds well at any scale μ below Λ. For the current numerical analysis, we shall choose a typical value of $y_b(m_t) \simeq y_t(m_t) \approx 3$, i.e., $|\mathcal{C}_L^{bb}| = |\mathcal{C}_R^{bb}| \simeq 3/\sqrt{2}$. In Fig. 16, we plot the production cross sections of h_b^0 or π_b^0 at the Tevatron and the LHC. This is similar to the charged top-pion production in Fig. 4, except the non-trivial differences in the Yukawa

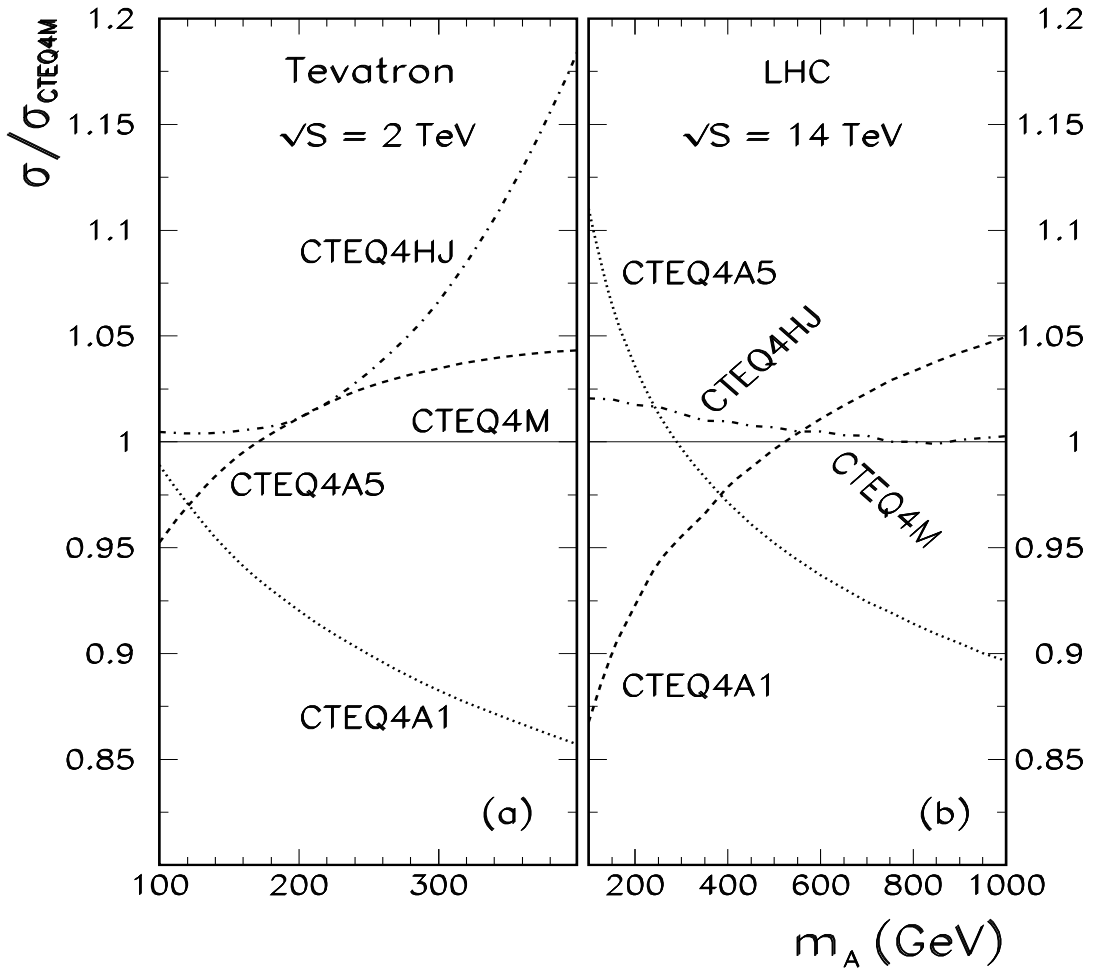

Figure 14: The ratios of NLO cross sections computed by four different sets of CTEQ4 PDFs relative to that by the CTEQ4M for neutral A^0-production in the MSSM with $\tan\beta = 40$, at the upgraded Tevatron (a) and the LHC (b).

couplings (due to the different tree-level values and the running behaviors) and the charm versus bottom parton luminosities.

5. Conclusions

In summary, we have presented the complete $O(\alpha_s)$ QCD corrections to the charged scalar or pseudo-scalar production via the partonic heavy quark fusion process at hadron colliders. We found that the overall NLO corrections to the $p\bar{p}/pp \to \phi^\pm$ processes are positive for m_ϕ above $\sim$150 (200) GeV and lie below $\sim$15 (10)% for the Tevatron (LHC) in the relevant range of m_ϕ (cf. Fig. 5). The inclusion of the NLO contributions thus justifies and improves our

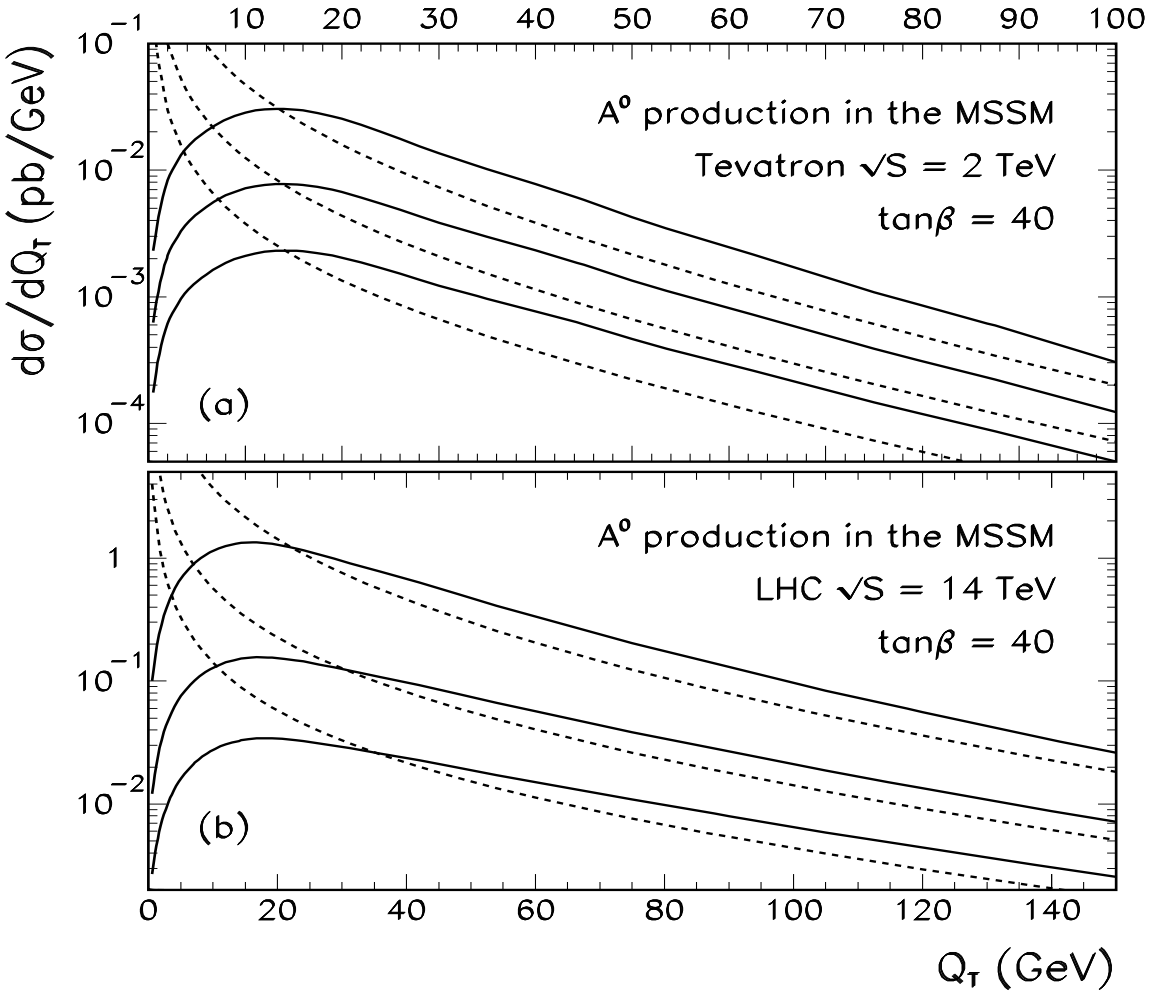

Figure 15: Transverse momentum distributions of pseudo-scalar A^0 produced via hadronic collisions, calculated in the MSSM with $\tan\beta = 40$. The resummed (solid) and $O(\alpha_s)$ (dashed) curves are shown for $m_A = 200$, 250, and 300 GeV at the upgraded Tevatron (a), and for $m_A = 250$, 400, and 550 GeV at the LHC (b).

recent LO analysis [1]. The uncertainties of the NLO rates due to the different PDFs are systematically examined and are found to be around 20% (cf. Table 1 and Fig. 6). The QCD resummation to include the effects of multiple soft-gluon radiation is also performed, which provides a better prediction of the transverse momentum (Q_T) distribution of the scalar $\phi^{0,\pm}$, and is important for extracting the experimental signals (cf. Fig. 7). We find that the resummed total rate differs from the $O(\alpha_s)$ rate only by a few percents which indicate that the size of the higher order corrections are likely much smaller than the uncertainty from the parton distribution functions (cf. Figs. 6 and 14). We confirm that the 2 TeV Tevatron (with a $2-10$ fb^{-1} integrated luminosity) is able to explore the natural mass range of the

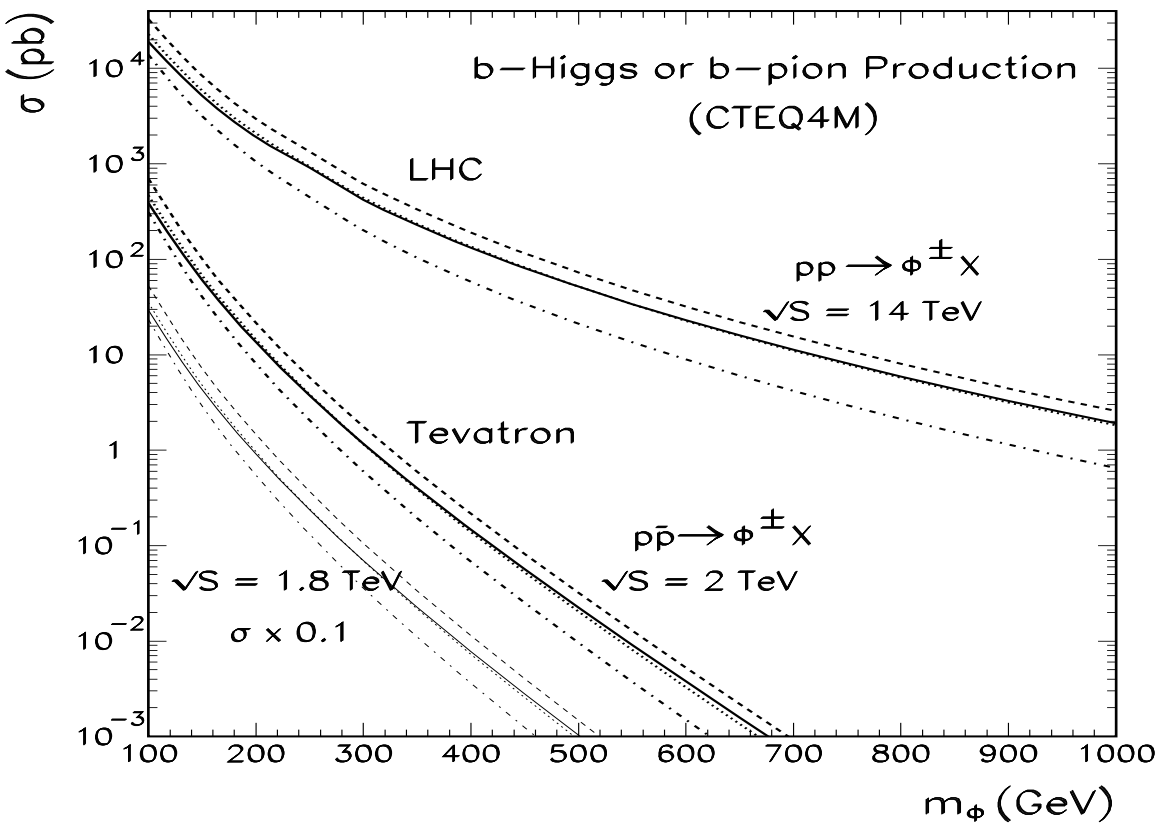

Figure 16: Cross sections for the neutral b-pion π_b^0 or b-Higgs h_b^0 production via the $b\bar{b}$-fusion in the TopC model at the Tevatron and the LHC. The NLO (solid), the $q\bar{q}'$ (dashed) and qg (dash-dotted) sub-contributions, and the LO (dotted) contributions with resummed running Yukawa coupling are shown. Since the qg cross sections are negative, they are multiplied by -1 in the plot. The cross sections at $\sqrt{S} = 1.8$ TeV are multiplied by 0.1 to avoid overlap with the $\sqrt{S} = 2$ TeV curves.

top-pions up to about 300–350 GeV in the TopC model [2, 11] for the typical t_R-c_R mixing of $K_{UR}^{tc} \sim 0.2 - 0.33$ [cf. eq. (11)]. Measuring the top polarization in the single-top event will further improve the signal identification. On the other hand, due to a possibly smaller $\phi^\pm$-b-c coupling in the 2HDM, we show that to probe the charged Higgs boson with mass above 200 GeV in this model may require a high luminosity Tevatron (with a $10 - 30$ fb^{-1} integrated luminosity). The LHC will further probe the charged Higgs boson of the 2HDM up to about $O(1)$ TeV via the single-top and $W^\pm h^0$ (or $W^\pm H^0$) production. The complementary roles of the tb and $W^\pm h^0$ channels in the different regions of the Higgs mass and the Higgs mixing angle α are demonstrated. We have also analyzed a direct extension of our NLO results to the neutral (pseudo-)scalar production via the $b\bar{b}$-fusion for the neutral Higgs bosons (A^0, h^0, H^0) in the MSSM with large tanβ, and for the neutral b-pion (π_b^0) or b-Higgs (h_b^0) in the TopC

model with $U(1)$-tilted large bottom Yukawa coupling. In comparison with the $\phi^0 b\bar{b}$ associate production [33], this inclusive ϕ^0-production mechanism provides a complementary probe for a neutral Higgs boson (with relatively large mass), whose decay products, e.g., in the $b\bar{b}$ or $\tau\tau$ channel, typically have high transverse momenta ($\sim m_\phi/2$) and can be effectively detected [35]. This is particularly helpful for the discovery reach of the Tevatron. Further detailed Monte Carlo analyses at the detector level should be carried out to finally conclude the sensitivity of the Tevatron Run-II and the LHC via this process.

At the final stage of writing up this manuscript, we became aware of a new preprint [40] which studied the QCD corrections for the neutral Higgs production $b\bar{b} \to H^0$ within the SM, and partially overlaps with our Sec. 4 as the pure NLO QCD correction is concerned. The overlapped part is in general agreement with ours except that we determine the counter term of the Yukawa coupling (expressed in terms of the relevant quark mass) by the on-shell scheme (cf. Refs. [26, 27]) while Ref. [40] used $\overline{\rm MS}$ scheme. After resumming the leading logarithms into the running mass or Yukawa coupling, the two results coincide. Note that the apparent large $O(\alpha_s)$ correction derived in Ref. [40] is due to the fact that it only includes the contribution from the $b\bar{b}$ sub-process, which is part of our complete $O(\alpha_s)$ contribution. The inclusion of the NLO contribution from the bg sub-process, which turns out to be negative and partially cancels the $b\bar{b}$ contribution, yields a typical size of $O(\alpha_s)$ correction to the production rate of a neutral Higgs boson produced via heavy quark fusion. The bg sub-process is identified as $O(1/\ln[m_H/m_b])$ instead of $O(\alpha_s)$ correction in Ref. [40].

Acknowledgments

We thank C.T. Hill for discussing the top-pion signature at the FermiLab Tevatron, H.E. Haber for discussing the charged Higgs production, W.K. Tung for discussing the heavy quark parton distribution functions, and J. Huston for discussing the CDF Run-Ib analysis on the new particle searches via the $b\bar{b}$ dijet mode [35]. We also thank the authors of Ref. [40] for confirming our comparison with their results, and explaining how they included the bg sub-process. This work is supported by the U.S. NSF under grant PHY-9802564.

Appendix

In this appendix, we present the individual NLO parton cross sections computed at $D = 4-2\epsilon$ dimensions. We note that, unlike the usual Drell-Yan type processes, the one-loop virtual contributions (cf. Fig. 1b-d) are not ultraviolet (UV) finite unless the new counter term from Yukawa coupling (related to the quark-mass renormalization, cf. Fig. 1e) is included.

A. Partonic processes $c\bar{b} \to \phi^+ X$

The spin- and color-averaged amplitude-square for the $c\bar{b} \to \phi^+ g$ process is

$$\overline{|\mathcal{M}|^2} = \frac{2\pi C_F}{3}\alpha_s \left(|\mathcal{C}_L|^2 + |\mathcal{C}_R|^2\right)\mu^{2\epsilon}\left[(1-\epsilon)\left(\frac{\widehat{t}}{\widehat{u}} + \frac{\widehat{u}}{\widehat{t}} + 2\right) + 2\frac{\widehat{s}\, m_\phi^2}{\widehat{t}\,\widehat{u}}\right]. \tag{22}$$

The individual contributions (from the virtual loop and real gluon emission) to the NLO partonic cross section are:

$$\begin{aligned}
\Delta\widehat{\sigma}^{\rm virtual}_{\rm loop} &= \widehat{\sigma}_0 \frac{\alpha_s C_F}{2\pi}\left(\frac{4\pi\mu^2}{Q^2}\right)^{\epsilon}\frac{\Gamma(1-\epsilon)}{\Gamma(1-2\epsilon)}\left[-\frac{2}{\epsilon^2} + \frac{2\pi^2}{3} - 2\right]\delta(1-\widehat{\tau}),\\
\Delta\widehat{\sigma}^{\rm virtual}_{\rm count} &= \widehat{\sigma}_0 \frac{\alpha_s C_F}{2\pi}(4\pi)^{\epsilon}\frac{\Gamma(1-\epsilon)}{\Gamma(1-2\epsilon)}\left[-\frac{3}{\epsilon} - \Omega\right]\delta(1-\widehat{\tau}),\\
\Delta\widehat{\sigma}^{\rm real}_{c\bar{b}} &= \widehat{\sigma}_0 \frac{\alpha_s C_F}{2\pi}\left(\frac{4\pi\mu^2}{Q^2}\right)^{\epsilon}\frac{\Gamma(1-\epsilon)}{\Gamma(1-2\epsilon)}\left[\frac{2}{\epsilon^2}\delta(1-\widehat{\tau}) + \frac{3}{\epsilon}\delta(1-\widehat{\tau}) - \frac{2}{\epsilon}P^{(1)}_{q\leftarrow q}(\widehat{\tau})C_F^{-1}\right.\\
&\quad \left. +4\left(1+\widehat{\tau}^2\right)\left(\frac{\ln(1-\widehat{\tau})}{1-\widehat{\tau}}\right)_+ - 2\frac{1+\widehat{\tau}^2}{1-\widehat{\tau}}\ln\widehat{\tau} + 2(1-\widehat{\tau})\right],\\
P^{(1)}_{q\leftarrow q}(\widehat{\tau}) &= C_F\left(\frac{1+\widehat{\tau}^2}{1-\widehat{\tau}}\right)_+ = C_F\left[\frac{1+\widehat{\tau}^2}{(1-\widehat{\tau})_+} + \frac{3}{2}\delta(1-\widehat{\tau})\right],
\end{aligned} \tag{23}$$

where the standard plus prescription $(\cdots)_+$ is given by

$$\int_0^1 d\alpha\, \xi(\alpha)\left[\chi(\alpha)\right]_+ = \int_0^1 d\alpha\, \chi(\alpha)\left[\xi(\alpha) - \xi(1)\right]. \tag{24}$$

In (23), the infrared $\frac{1}{\epsilon^2}$ poles cancel between $\Delta\widehat{\sigma}^{\rm virtual}_{\rm loop}$ and $\Delta\widehat{\sigma}^{\rm real}_{c\bar{b}}$. The term $\Delta\widehat{\sigma}^{\rm virtual}_{\rm loop}$ from the virtual loop actually contains two types of $\frac{1}{\epsilon}$ poles inside $[\cdots]$: $\frac{3}{\epsilon_{UV}} + \frac{3}{\epsilon_{IR}}$ with $\epsilon_{UV} = -\epsilon_{IR} \equiv \epsilon = (4-D)/2 > 0$. Also, the $-\frac{3}{\epsilon}$ pole inside the Yukawa counter-term contribution $\Delta\widehat{\sigma}^{\rm virtual}_{\rm count}$ is ultraviolet while the $+\frac{3}{\epsilon}$ pole inside $\Delta\widehat{\sigma}^{\rm real}_{c\bar{b}}$ is infrared (IR). We see that the contribution

$\Delta\widehat{\sigma}^{\rm virtual}_{\rm count}$ from the counter term of the Yukawa coupling is crucial for cancelling the UV divergence from $\Delta\widehat{\sigma}^{\rm virtual}_{\rm loop}$ (which is absent in the usual Drell-Yan type processes), while the soft $\frac{1}{\epsilon}$ divergences between $\Delta\widehat{\sigma}^{\rm virtual}_{\rm loop}$ and $\Delta\widehat{\sigma}^{\rm real}_{c\bar{b}}$ cancel. Finally, the $\frac{1}{\epsilon}$ collinear singularity inside $\Delta\widehat{\sigma}^{\rm real}_{c\bar{b}}$ will be absorbed into the re-definition of the PDF via the quark-quark transition function $P^{(1)}_{q\leftarrow q}(\widehat{\tau})$. All the finite terms are summarized in Eq. (4).

B. Partonic processes $gc, g\bar{b} \to \phi^+ X$

The spin- and color-averaged amplitude-square for the $gc, g\bar{b} \to \phi^+ X$ process is

$$\overline{|\mathcal{M}|^2} = \frac{\pi\alpha_s}{3(1-\epsilon)}\left(|\mathcal{C}_L|^2+|\mathcal{C}_R|^2\right)\mu^{2\epsilon}\left[(1-\epsilon)\left(\frac{\widehat{s}}{-\widehat{t}}+\frac{-\widehat{t}}{\widehat{s}}-2\right)-2\frac{\widehat{u}\,m_\phi^2}{\widehat{s}\,\widehat{t}}\right]. \tag{25}$$

The $O(\alpha_s)$ partonic cross section for the quark-gluon fusions is given by:

$$\begin{aligned}
\Delta\widehat{\sigma}^{\rm real}_{cg,\bar{b}g} &= \widehat{\sigma}_0\frac{\alpha_s C_F}{2\pi}\left(\frac{4\pi\mu^2}{Q^2}\right)^{\epsilon}\left[\left(-\frac{1}{\epsilon}\frac{\Gamma(1-\epsilon)}{\Gamma(1-2\epsilon)}+\ln\frac{(1-\widehat{\tau})^2}{\widehat{\tau}}\right)P^{(1)}_{q\leftarrow g}(\widehat{\tau})+\frac{1}{4}(-3+7\widehat{\tau})(1-\widehat{\tau})\right],\\
P^{(1)}_{q\leftarrow g}(\widehat{\tau}) &= \frac{1}{2}\left[\widehat{\tau}^2+(1-\widehat{\tau})^2\right],
\end{aligned} \tag{26}$$

where it is clear that the collinear $\frac{1}{\epsilon}$ singularity will be absorbed into the re-definition of the PDF via the gluon-splitting function $P^{(1)}_{q\leftarrow g}(\widehat{\tau})$. The final result is finite and is given in Eq. (4).

References

1. H.-J. He and C.-P. Yuan, Phys. Rev. Lett. (1999), in press, hep-ph/9810367.
2. C.T. Hill, hep-ph/9702320 and hep-ph/9802216.
3. For a review, G. Cvetic, Rev. Mod. Phys. **71** (1999) 513, hep-ph/9702381.
4. T.P. Cheng and M. Sher, Phys. Rev. D**35** (1987) 3484; M. Sher and Y. Yuan, Phys. Rev. D**44** (1991) 1461; L.J. Hall and S. Weinberg, Phys. Rev. D**48** (1993) R979.
5. L. Reina, hep-ph/9712426; M. Sher, hep-ph/9809590; D. Atwood, L. Reina, and A. Soni, Phys. Rev. D**54** (1996) 3296; D**55** (1997) 3156; J.L. Diaz-Cruz, et al, *ibid*, D**51** (1995) 5263; and references therein.
6. H.E. Haber and G.L. Kane, Phys. Rep. **117** (1985) 75.
7. H.E. Haber, Nucl. Phys. Proc. Suppl. **62** (1998) 469; and references therein.
8. R.M. Barnett, H.E. Haber, and D.E. Soper, Nucl. Phys. **B**306 (1988) 697.
9. M.A.G. Aivazis, J.C. Collins, F.I. Olness, and W.K. Tung, Phys. Rev. D**50** (1994) 3102;
10. J.C. Collins, Phys. Rev. D**58** (1998) 094002.
11. C.T. Hill, Phys. Lett. B**345** (1995) 483; G. Buchalla, G. Burdman, C.T. Hill, and D. Kominis, Phys. Rev. D**53** (1996) 5185.
12. G. Altarelli, R.K. Ellis, and G. Martinelli, Nucl. Phys. **B**157 (1979) 461.
13. N. Gray, et al, Z. Phys. C**48** (1990) 673; S. Narison, Phys. Lett. B**341** (1994) 73.
14. E.g., M.E. Peskin and D.V. Schroeder, *An Introduction to Quantum Field Theory,* Addison-Wesley Publishing Company, 1995; Particle Data Group, European Phys. J. **C3** (1998) 1.
15. B. Balaji, Phys. Lett. B**393** (1997) 89.
16. W. Hollik, talk given at 29th International Conference on High-Energy Physics (ICHEP 98), Vancouver, Canada, 23-29 Jul 1998, hep-ph/9811313; J. Erler and P. Langacker, in the Proceedings of the 5th International WEIN Symposium, Santa Fe, NM, June 14-21, 1998, hep-ph/9809352 and private communications; G. Altarelli, hep-ph/9811456.
17. G. Burdman and D. Kominis, Phys. Lett. B**403**, 101 (1997).
18. H. Pagels and S. Stokar, Phys. Rev. D**20** (1979) 2947.
19. L. Wolfenstein, Phys. Rev. Lett. **51** (1983) 1945.

20. H.L. Lai, et al., (CTEQ Collaboration), Phys. Rev. D**55** (1997) 1280.
21. J. Collins, F. Wilczek, and A. Zee, Phys. Rev. D**18** (1978) 242.
22. C. Balázs and C.-P. Yuan, Phys. Rev. D**56** (1997) 5558.
23. J. Collins and D. Soper, Nucl. Phys. B**193** (1981) 381; B**213** (1983) 545(E); Nucl. Phys. B**197** (1982) 446; J. C. Collins, D. Soper, and G. Sterman, Phys. Lett. B**109** (1982) 388; Nucl. Phys. B**223** (1983) 381; Phys. Lett. B**126** (1983) 275; Nucl. Phys. B**250** (1985) 199.
24. V.N. Gribov and L.N. Lipatov, Yad. Phys. **15** (1972) 781 (Sov. J. Nucl. Phys. **15** (1972) 438); L.N. Lipatov, Yad. Phys. **20** (1975) 181 (Sov. J. Nucl. Phys. **20** (1975) 94); Yu.L. Dokshitzer, Sov. Phys. JETP **46** (1977) 641;
25. G. Altarelli and G. Parisi, Nucl. Phys. **B126** (1977) 298; G. Altarelli, Phys. Rep. **81** (1982) 1.
26. A. Djouadi and P. Gambino, Phys. Rev. **D**51 (1995) 218; A. Djouadi, M. Spira, and P.M. Zerwas, Z. Phys. C**70** (1996) 427.
27. C.S. Li and R.J. Oakes, Phys. Rev. **D**43 (1991) 855.
28. T. Tait and C.-P. Yuan, hep-ph/9710372.
29. S.L. Glashow and S. Weinberg, Phys. Rev. D**15** (1977) 1958.
30. G. Cvetic, S.S. Hwang, and C.S. Kim, Phys. Rev. D**58** (1998) 116003.
31. A.K. Grant, Phys. Rev. D**51** (1995) 207.
32. D. Atwood, L. Reina, and A. Soni, Phys. Rev. D**54** (1996) 3296, and L. Reina, private communication on the issue of R_b in 2HDM.
33. C. Balázs, J.L. Diaz-Cruz, H.-J. He, T. Tait, and C.-P. Yuan, Phys. Rev. D**59** (1999) 055016, hep-ph/9807349; J.L. Diaz-Cruz, H.-J. He, T. Tait, and C.-P. Yuan, Phys. Rev. Lett. **80** (1998) 4641.
34. A. Djouadi, J. Kalinowki, and M. Spira, Comput. Phys. Commun. **108** (1998) 56.
35. F. Abe, et al, (CDF collaboration), "*Search for new particles decaying to $b\bar{b}$ in $p\bar{p}$ collisions at $\sqrt{s} = 1.8\ TeV$*", Phys. Rev. Lett. **82** (1999) 2038.
36. J. Dai, J. Gunion, and R. Vega, Phys. Lett. B**345** (1995) 29; B**387** (1996) 801.
37. D. Choudhury, A. Datta, and S. Raychaudhuri, hep-ph/9809552.
38. M. Drees, M. Guchait, and P. Roy, Phys. Rev. Lett. **80** (1998) 2047; **81**, 2394(E); M. Carena, S. Mrenna, and C.E.M. Wagner, hep-ph/9808312.

39. R. Hempfling, Phys. Rev. D**49** (1994) 6168; L.J. Hall, R. Rattazzi, and U. Sarid, Phys. Rev. D**50** (1994) 7048; M. Carena, M. Olechowski, S. Pokorski, and C.E.M. Wagner, Nucl. Phys. B**426** (1994) 269. D.M. Pierce, J.A. Bagger, K. Matchev, and R.J. Zhang, Nucl. Phys. B**491** (1997) 3, and references therein.
40. D. Dicus, T. Stelzer, Z. Sullivan, and S. Willenbrock, hep-ph/9811492.